Bioactive Materials 45 (2025) 181–200

Contents lists available at ScienceDirect

Bioactive Materials

journal homepage: www.keaipublishing.com/en/journals/bioactive-materials

Engineering aortic valves via transdifferentiating fibroblasts into valvular endothelial cells without using viruses or iPS cells

Peng Tang [a,1], Fuxiang Wei [a,1], Weihua Qiao [b,1], Xing Chen [b], Chenyang Ji [a], Wanzhi Yang [a], Xinyu Zhang [a], Sihan Chen [a], Yanyan Wu [a], Mingxing Jiang [a], Chenyu Ma [a], Weiqiang Shen [a], Qi Dong [a], Hong Cao [b], Minghui Xie [b], Ziwen Cai [b], Li Xu [b], Jiawei Shi [b], Nianguo Dong [b,**], Junwei Chen [a,*], Ning Wang [c,***]

[a] Key Laboratory of Molecular Biophysics of the Ministry of Education, Hubei Bioinformatics and Molecular Imaging Key Laboratory, Laboratory for Cellular Biomechanics and Regenerative Medicine, Department of Biomedical Engineering, College of Life Science and Technology, Huazhong University of Science and Technology, Wuhan, Hubei, 430074, China

[b] Department of Cardiovascular Surgery, Union Hospital, Tongji Medical College, Huazhong University of Science and Technology, Wuhan, 430022, China

[c] Institute for Mechanobiology, Department of Bioengineering, College of Engineering, Northeastern University, Boston, MA, 02115, USA

ARTICLE INFO

Keywords:
Transdifferentiation
Valvular endothelial cells
Tissue engineered aortic valves
Soluble factors, Substrate stiffness

ABSTRACT

The technology of induced pluripotent stem cells (iPSCs) has enabled the conversion of somatic cells into primitive undifferentiated cells via reprogramming. This approach provides possibilities for cell replacement therapies and drug screening, but the potential risk of tumorigenesis hampers its further development and *in vivo* application. How to generate differentiated cells such as valvular endothelial cells (VECs) has remained a major challenge.

Utilizing a combinatorial strategy of selective soluble chemicals, cytokines and substrate stiffness modulation, mouse embryonic fibroblasts are directly and efficiently transdifferentiated into induced aortic endothelial cell-like cells (iAECs), or human primary adult fibroblasts are transdifferentiated into induced valvular endothelial cell-like cells (hiVECs), without expressing pluripotency stem cell markers. These iAECs and hiVECs express VEC-associated genes and proteins and VEC-specific marker NFATC1 and are functional in culture and on decellularized porcine aortic valves, like mouse aortic endothelial cells or human primary aortic valvular endothelial cells. The iAECs and hiVECs seeded on decellularized porcine aortic valves stay intact and express VEC-associated proteins for 60 days after grafting into abdominal aorta of immune-compromised rats. In contrast, induced pluripotent stem cells (iPSCs) are less efficient in differentiating into VEC-like cells and pluripotency marker Nanog is expressed in a small subpopulation of iPSC-derived VEC-like cells that generate teratomas in SCID mice whereas hiVECs derived from transdifferentiation do not generate teratomas *in vivo*. Our findings highlight an approach to efficiently convert fibroblasts into iAECs and hiVECs and seed them onto decellularized aortic valves for safely generating autologous tissue-engineered aortic valves without using viruses or first reprogramming the cells into pluripotent stem cells.

Peer review under responsibility of KeAi Communications Co., Ltd.

* Corresponding author.

** Corresponding author.

*** Corresponding author.

E-mail addresses: 854087174@qq.com (P. Tang), weihust@hotmail.com (F. Wei), weihua_qiao@hust.edu.cn (W. Qiao), 1747155541@qq.com (X. Chen), 1654875704@qq.com (C. Ji), ema456123789@qq.com (W. Yang), 1624413165@qq.com (X. Zhang), chensihan_shirly@qq.com (S. Chen), 1921335284@qq.com (Y. Wu), 502078696@qq.com (M. Jiang), 980574163@qq.com (C. Ma), 848452868@qq.com (W. Shen), 1306584051@qq.com (Q. Dong), caohonghuster@163.com (H. Cao), 1018411891@qq.com (M. Xie), 171961014@qq.com (Z. Cai), whunionxl@163.com (L. Xu), shijiawei@hotmail.com (J. Shi), dongnianguo@hotmail.com (N. Dong), chenjunwei@hust.edu.cn (J. Chen), ni.wang@northeastern.edu (N. Wang).

[1] These authors contributed equally to this work.

https://doi.org/10.1016/j.bioactmat.2024.11.018

Received 31 July 2024; Received in revised form 30 October 2024; Accepted 14 November 2024

1. Introduction

Valvular heart disease (VHD) is one of the main causes of death worldwide with the number of affected people constantly growing. Valve replacement is the most used form of treatment for patients with end-stage VHD and hundreds of thousands of heart valve replacement surgeries are performed annually worldwide [1,2]. Various methods and strategies have been developed to generate prosthetic heart valves. For example, a jet spinning process is shown to allow for rapid manufacturing of biohybrid scaffolds for biomimetic heart valve replacement [3]. However, bio-prosthetic and mechanical valves do not have any capacity for growth or regeneration, representing serious challenges for pediatric patients [4]. Therefore, creating tissue engineered heart valves to serve as an alternative to bio-prosthetic or mechanical valves has become an urgent necessity [5].

The native heart aortic valves contain two primary cell populations: valvular endothelial cells (VECs) and valvular interstitial cells (VICs). Both types of cells play critical roles in the development, maintenance, and repair of heart valves [6]. Recently it is shown that post TAVR (transcatheter aortic valve replacement) serum reduces activation of VICs in patients [7]. TNF (tumor necrosis factor)-α and IL (interleukin)-1β from M1 macrophages suppress activated VIC-mediated fibrosis and eventual calcification of valve tissues [8]. Swine VECs and aortic endothelial cells (AECs) exhibit different transcriptional and proliferative profiles on various extracellular matrices [9] and VECs orient circumferentially on leaflet surfaces [10]. VECs also exhibit location-specific differences between fibrosa and ventricularis [11,12]. Several strategies have been attempted in recellularization of decellularized heart valves [13,14], but it remains challenging to identify optimal culture protocols using various chemical and mechanical modulators. Creating VEC-like cells and integrating them into functional valve scaffolds are critical for manufacturing autologous valves that can grow and regenerate in pediatric patients.

Induced pluripotent stem cells (iPSCs) can be derived from various cell lineages [15–18]. These cells are able to differentiate into many cell lineages, including hepatocytes, cardiomyocytes, neural precursors, and endothelial cells [19–22]. However, the problems of tumorigenic propensity and inefficient cell production have limited clinical application of iPSCs [23–25]. Direct lineage reprograming, i.e., transdifferentiation, is an alternative for the source of VECs. A report has shown successful *in vivo* reprogramming of adult pancreatic exocrine cells to beta-cells by combination of three transcription factors [26]. Approaches that utilize adenovirus or lentivirus have also been developed for generating target cells through reprogramming with cell-type-specific transcription factors [27–30], with the caveat of potential risks of introducing viruses into the recipients. Therefore, seeking an alternative safe and efficient method becomes urgent and necessary. In this study we report a strategy to directly convert differentiated fibroblasts into iAECs and hiVECs without virus utilization and genetic manipulation.

2. Materials and methods

2.1. Isolation of primary human VECs and fibroblasts

Human primary adult aortic valvular endothelial cells were collected from the explanted hearts of patients who underwent heart transplantation for dilated cardiomyopathy, following a previously established protocol [31]. Exclusion criteria included bicuspid aortic valves, valves with moderate-to-severe aortic valve regurgitation, infective endocarditis, congenital valve disease, and rheumatic aortic valvulopathy. After the heart valve was digested with type I collagenase (MERCK, Cat No.SCR103, Germany) of 2 mg per mL at 37 °C for 20 min, the VECs on the surface of the valve were gently scraped with a throat swab, purified by magnetic beads, then cultured in human endothelial growth medium-2 (EGM-2, Lonza, CC-3162) added with 5 μM SB431542 (Selleck, S1067) (5 % CO_2, 37 °C) *in vitro* [32]. Human primary adult dermal fibroblasts were isolated from foreskin after posthectomy. Samples were obtained from 5 human biopsy donors. Each donor donated a piece of foreskin after surgical operation and the human primary dermal fibroblasts from one foreskin were used for one batch of transdifferentiation. The isolation and purification method was used according to a published paper [33].

The protocol for this study complied with the Declaration of Helsinki and was approved by the Tongji Medical College Institutional Review Board and the Ethics Committee of Tongji Medical College (Ethics review number: S999-2016), Huazhong University of Science and Technology. Written informed consents were obtained from all patients.

2.2. Cell culture

Mouse embryonic fibroblast cells, NIH/3T3, mouse aortic endothelial cells (MAECs), human umbilical vein endothelial cells (HUVECs), human embryonic fibroblast cells M − 20, human adult primary dermal fibroblasts (HDF), human primary aortic valve endothelial cells (HAVECs), human induced pluripotent stem cell line PGP1, and mouse embryonic stem cell (ESC) line (OGTR1) were cultured and maintained in each specific type of medium. The OGTR1 ESC line was cultured as described previously [34]. The details are shown in Appendix A. Supplementary data. Culture medium was changed daily. All cells were randomly assigned to experimental groups. The potential contamination of mycoplasma was constantly monitored by examining DNA DAPI staining and no contamination was found in any of the cell lines.

2.3. Mouse iAECs generation

To generate mouse induced AEC-like cells (iAECs), 3T3 fibroblasts were seeded on fibronectin-coated plates or PDMS and 5-Azacytidine were added for 24 h (day 1). Then the medium was changed to induction medium containing basal medium (E6 medium), BMP4, CHIR99021 for 4 additional days. On day 5, medium was changed to induction medium including basal medium with VEGF, DAPT, PIGF, HGF and 8-Br-cAMP for 6 additional days. On day 11, iAECs were resuspended and seeded on PGG-crosslinked decellularized porcine heart valves for 10 days, medium changed to complete mouse endothelial cell medium containing VEGF, SB431542, 8-Br-cAMP. The cells were cultured in mouse endothelial cell medium added with VEGF and SB431542 for cellular expansion. The details are shown in Appendix A. Supplementary data. After establishing this protocol, iAECs were successfully generated in all succeeding experiments except for a few cases, which may be due to the quality of the PGG-crosslinked decellularized porcine heart valves.

2.4. Human hiVECs generation

To generate induced human VEC-like cells (hiVECs), human M − 20 fibroblast cell lines were seeded on Matrigel-coated plates and 5-Azacytidine were added for 24 h (day 1). Then the medium was changed to induction medium containing basal medium (E6 medium) or N2/B27 medium human BMP4, WNT3A for one day. On day 2, medium was changed to induction medium including basal medium or N2/B27 medium with human BMP4, bFGF for one day. On day 3 medium was changed to induction medium including basal medium (E6 medium) or StemPro-34 serum-free medium with VEGF, bFGF for 6 additional days. On day 9, FACS analysis and MACS sorting were performed, purified cells were cultured in EGM-2 added with VEGF, SB431542 and 8-Br-cAMP for cellular expansion for about 4 days. On day 13, purified hiVECs were seeded on PGG-crosslinked decellularized porcine heart valves for 7 additional days in the EGM2 culture medium containing VEGF, SB431542 and 8-Br-cAMP. After establishing this protocol, hiVECs were successfully generated in all succeeding experiments.

Furthermore, human primary adult fibroblasts were used to generate human induced VEC-like cells (hiVECs). Human adult primary dermal

fibroblasts (HDF) were seeded on fibronectin-coated plates or PDMS and 5-Azacytidine were added for 24 h (day 1). Then the medium was changed to induction medium containing basal medium (E6 medium) or N2/B27 medium, BMP4, CHIR99021 for 4 additional days. On day 5, medium was changed to induction medium including basal medium (E6 medium) or StemPro-34 serum-free medium with VEGF, DAPT, PIGF, HGF and 8-Br-cAMP for 8 additional days. On day 13, purified hiVECs were seeded on PGG-crosslinked decellularized porcine heart valves for 7 additional days in the EGM-2 medium containing VEGF, SB431542 and 8-Br-cAMP. Human M-20 cells were reprogrammed into iPSCs according to the published method [35]. iPSC-derived human induced VEC-like cells (iPSC-hiVECs) were produced using M-20 derived human iPSCs or PGP1 human iPSCs according to the published protocol [36]. The details are shown in Appendix A. Supplementary data. The success rate of this protocol was ~72 % for all experiments and the unsuccessful ones appeared to be due to poorly crosslinked decellularized porcine heart valves.

2.5. Animals

Six-week-old nude male rats were obtained from Charles River (Beijing, China). The rats were randomly assigned to the negative control group or the treated groups; each group had six rats; the rats in each group were growing and gaining weight during the 30-day and the 60-day experiments. Four-week-old female NOD-SCID mice were obtained from Charles River (Beijing, China). The mice were randomly assigned to three treated groups and each group had five mice. The experimentalists were blinded by the expected outcome of the treatment. All animals received humane care in compliance with the Principles of Laboratory Animal Care Formulated by the National Society of Medical Research and the Guide for the Care and Use of Laboratory Animals by National Research Council (US). The protocol was approved by the Animal Care and Use Committee of Huazhong University of Science and Technology.

2.6. Teratoma formation assay

Two million viable purified hiVEC, M-20-iPSC-hiVEC and iPSC-hiVEC in 0.1 ml PBS were injected into NOD-SCID mice subcutaneously. Mice conditions and tumor formation were monitored regularly throughout the experiments. They were humanely sacrificed after 4–6 weeks and teratomas were isolated. These teratomas were fixed with 4 % paraformaldehyde in PBS at 4 °C overnight and further processed for Hematoxylin and Eosin (H&E) and immunofluorescence staining, anti-Nestin (1:200, chicken monoclonal, Novus, NB100-1604) and anti-Brachyury (1:1000, rabbit monoclonal, Abcam, ab209665) and anti-Gata6 (1:200, rabbit monoclonal, Abcam, ab22600) antibodies were used to test teratogenesis.

2.7. PDMS fabrication

PDMS were fabricated according to the specification of SYLGARD184 Silicone Elastomer Kit (Dow Corning Corporation, Midland, MI). The base: curing agent ratios (w/w) of 5:1, 10:1, 20:1, and 40:1 was used for sake of different stiffness. The Young's moduli of 5:1 PDMS, 10:1 PDMS, 20:1 PDMS, and 40:1 PDMS were 2.6 MPa, 2.1 MPa, 1.0 MPa, and 0.1 MPa, respectively [37]. For each stiffness, base and curing agents were thoroughly mixed and degassed under vacuum for 30 min. Then, the mixture was poured into a 24-well plate, stored at 60 °C for 24 h for curing, and polymerized at room temperature for 24 h. PDMS plates were sterilized by 75 % ethanol for 30 min and exposed to ultraviolet light for 30min. All the sterilized PDMS plates were sealed and stored at room temperature until use.

2.8. Quantification of circularity index

To quantify the shape of different cells in our experiments, circularity index was calculated by tracing the perimeter of the cell and determining the projected area of the cell. The circularity of colonies was calculated using the formula of 4π (area) divided by perimeter squared. A perfect circle has a value of 1.0.

2.9. RNA extraction and quantitative polymerase chain reaction

Total mRNA was isolated from the cells using the Trizol reagent according to the supplier's instruction (Invitrogen), and quantitative polymerase chain reaction (PCR) was performed with the use of HiScript II One Step qRT-PCR SYBR Green Kit (Vazyme). Genes associated with the fibroblast phenotype, *Vimentin, S100a4, α-SMA* and EC phenotype, *Flk1, CD144, CD31*, *Sox18, Sox17, Fli1, Elk3, Erg* and iPSC phenotype, *TRA-1-81, SSEA1, Nanog, OCT4* and *SOX2* were analyzed with the data normalized to GAPDH housekeeping gene and expressed as relative fold changes with the ΔCt method of analysis. Primer information of all genes was listed in Tables S1 and S2.

2.10. Flow cytometry

For transdifferentiation efficiency quantification, the iAEC or hiVECs were dissociated into single cells with TrypLE (Life Technologies) for 3 min at 37 °C, washed with 1 × phosphate-buffered saline (PBS, Hyclone) containing 5 % bovine serum albumin, and passed through a 70-μm cell strainer. Murine cells were incubated with primary antibodies anti-CD144 (VE-cadherin) (1:100, mouse monoclonal, BioLegend, catalog # 138006) and anti-CD31 (1:100, mouse monoclonal, BioLegend, catalog # 102524) for 30 min, Homo sapiens cells were incubated with primary antibodies anti-CD144 (VE-cadherin) (1:20, mouse monoclonal, BioLegend, catalog # 348514) and anti-CD31 (1:20, mouse monoclonal, BioLegend, catalog # 303106) for 30 min, then washed with EDTA buffer once. Isotype-matched antibody served as negative control. Cells were analyzed by using Beckman™ CytoFLEX flow cytometry. For histone methylation analysis, cells were fixed with 4 % paraformaldehyde at 4 °C for 30min, then permeabilized by 0.5 % Triton X-100 at room temperature for 15min; after that the cells were incubated with anti-H3K9me3 primary antibody (1:50, Cell signaling, rabbit monoclonal, #13969), anti-H3K27me3 primary antibody (1:200, Cell signaling, rabbit monoclonal, #9733), anti-H3K4me3 primary antibody (1:1000, Cell signaling, rabbit monoclonal, #9751) at 4 °C for 1.5 h, anti-Rabbit secondary antibody(Invitrogen, donkey polyclonal, 1:200, A-21207) at 4 °C for 1 h. For TRA-1-81 and SSEA1 analysis of iPSCs, cells were fixed with 4 % paraformaldehyde at 4 °C for 30 min and then incubated with anti-TRA-1-81 primary antibody (1:1600, Cell signaling, mouse monoclonal, #4745) and anti-SSEA1 primary antibody (1:1600, Cell signaling, mouse monoclonal, #4744) at 4 °C for 1.5 h, anti-mouse secondary antibody (Invitrogen, goat polyclonal, 1:200, A-11001) at 4 °C for 1 h. Isotype-matched antibody served as negative control. Beckman CytExpert was used for sample analysis.

2.11. Immunofluorescence

Adherent cells were fixed with 4 % paraformaldehyde and subjected to immunofluorescence using standard protocols and the following primary antibodies: anti-CD31 (1:100, rat monoclonal, Abcam, ab7388) and anti-CD144 (VE-Cadherin) (1:100, rabbit polyclonal, Abcam, ab205336) for murine cells; anti-CD31 (1:200, mouse monoclonal, Abcam, ab9498), anti-CD144 (VE-Cadherin) (1:200, rabbit-monoclonal, Abcam, ab33168) for homo sapiens cells. Anti-TRA-1-81 (mouse monoclonal, Cell signaling, #4745, 1:500), Anti-SSEA1 (mouse monoclonal, Cell signaling, #4744, 1:500), Anti-Oct4 (mouse monoclonal, Abcam, ab181557, 1:200) and anti-Nanog antibody (rabbit polyclonal, Abcam, ab106465, 1:200). Anti-Phospho-VEGF Receptor 2 (Rabbit

monoclonal, Cell signaling, #2478, 1:200), anti-CD62E (Rabbit monoclonal, Abcam, ab18981, 1:200), anti-CD62P (mouse monoclonal, Abcam, ab6632, 1:200), anti-Vimentin (Rabbit monoclonal, Abcam, ab92547, 1:500), anti-brachyury (Rabbit monoclonal, Abcam, ab209665, 1:500), anti-sox17 (Rabbit monoclonal, Abcam, ab224637, 1:500), anti-Fli1 (Rabbit monoclonal, Abcam, ab133485, 1:700), NFATC1 (Rabbit monoclonal, Thermo, #PA5-79730, 1:500), anti-NRP1 (phospho-Thr916) (Rabbit monoclonal, Biorbyt, orb101815, 1:200), anti- HGFR/c-MET [p Tyr1234, p Tyr1235] Antibody (Rabbit monoclonal, NOVUS, AF2480, 1:40), Goat anti-Rabbit IgG (H + L) Highly Cross-Adsorbed Secondary Antibody, Alexa Fluor Plus 594 (goat polyclonal, Thermo, A32740, 1:1000) and Goat anti-Mouse IgG (H + L) Highly Cross-Adsorbed Secondary Antibody, Alexa Fluor Plus 488(goat polyclonal, Thermo, A32723, 1:1000). AlexaFluor 488- or 594-conjugated secondary antibodies (Life Technologies, 1:1000) specific to the appropriate species were used to detect bound primary antibodies. Nuclei were counterstained with DAPI (Biosharp, 1:1000). Images were captured using a Leica DMI6000B microscopic imaging system. Images were analyzed with Image J software.

2.12. Western blotting

Total cellular protein was extracted from cultured cells after homogenization in a RIPA lysis buffer containing protease inhibitor and phosphatase inhibitor cocktails (both from Beyotime). Total lysates were separated by SDS-PAGE and transferred onto nitrocellulose membranes (Millipore). Membranes were incubated with primary antibodies to GAPDH (1:1000, Abclonal, #103386), CD144 (1:1000, Abcam, ab33168), CD31 (1:1000, Abcam, ab9498 for homo sapiens cells), CD31 (1:1000, Abcam, ab24590) and H3K9me3 (1:1000, Cell Signaling, #13969) followed by incubation with Anti-rabbit IgG (H + L) (DyLight (TM))800 4xPEG Conjugate (Cell Signaling, #5151P) and Anti-mouse IgG (H + L) (DyLight (TM))800 4xPEG Conjugate (Cell Signaling, #5257P) specific to the appropriate species. Enhanced chemiluminescent (ECL) substrate (SuperSignal West Femto Substrate; Thermo Scientific) was used to detect bound antibody. Bands were visualized into UVP ChemiDoc-It 510 Imager System, scanned, and quantified with Image J. The signal intensity was normalized to GAPDH expression.

2.13. MACS sorting

hiVECs, M-20-iPSC-hiVECs, PGP1-hiVECs and HDF-hiVECs were purified with magnetic-activated cell sorting (MACS) and anti-CD144 (Miltenyi Biotec, #130-097-857) magnetic beads according to the manufacturer's recommended protocol. Briefly, 10^7 cells were resuspended in 70 μl of separation buffer (phosphate-buffered saline (PBS), (Hyclone) containing 0.5 % bovine serum albumin (BSA) and 2 mM EDTA (both from Sigma-Aldrich)), incubated for 15 min at 4 °C with 20 μl of anti-CD144 Microbeads per 80 μl of cell suspension, washed by adding 1 ml of separation buffer and centrifuged at 300×*g* for 10 min. Cells were resuspended in 500 μl of separation buffer and passed through 30-μm nylon mesh (Miltenyi Biotec, # 130-041-407) to remove cell clumps which might clog the column. LS columns (Miltenyi Biotec, # 130-042-401) were rinsed with buffer (Diluting MACS BSA Stock Solution (Miltenyi Biotec, # 130-091-376) 1:20 with autoMACS® Rinsing Solution (Miltenyi Biotec, # 130-091-222)) before usage. Then the cell suspension was applied onto the LS Column placed in the magnetic field of a MACS Separator (Miltenyi Biotec). The flow-through was collected as the unlabelled negative fraction. The column was washed three times with 500 μl of buffer and the retained magnetically labelled cells were flushed out with 1 ml of buffer as the positive fraction.

2.14. In vitro vascular tube formation assay

100 μL Matrigel (8.7 mg per mL; ~1 kPa in modulus [38].) per well was placed into each well of a 24-well plate and incubated at 37 °C for 1 h to solidification. 5.0×10^4 cells were suspended in 500 μL of mouse endothelial cell medium for murine cells or endothelial growth medium-2 (EGM-2) for homo sapiens cells, and then seeded onto the Matrigel. Images were quantified for tube numbers and branch lengths by Ibidi Systems Software. The tubes were labelled by Calcein-AM (DojinDo, C542) and then whole blood labelled by DiD was added to the culture medium (Beyotime, C1039) and perfused into the tube structures, following the published procedures [39]. The samples were visualized using DMI6000B Leica microscopic imaging system. Lumen formation was observed under Hitachi HT7700 scanning transmission electron microscope.

2.15. DiI-Ac-LDL uptake assay

Uptakes of acetylated low-density lipoprotein (Ac-LDL) were evaluated by incubating cells with DiI-Ac-LDL (Yeasen) at 1:100 dilution for 4 h. The cells were washed with phosphate-buffered saline (PBS) and then nuclei were counterstained with Hoechst 33258 (Meilun Biotechnology Co.) for 10 min. The mean fluorescence intensity of the whole cells was quantified using imaging analysis software (Image J).

2.16. In vitro VEGF stimulation assay

Mouse and human fibroblasts, iAECs, hiVECs, MAEC, HUVEC and HAVEC were exposed to 50 ng per mL VEGF of the corresponding species for 15 min. Then the cells were fixed with 4 % paraformaldehyde and subjected to immunofluorescence using standard protocols and the following primary antibodies: Anti-Phospho-VEGF Receptor 2 (Rabbit monoclonal, Cell signaling, #2478, 1:200); Goat anti-Rabbit IgG (H + L) Highly Cross-Adsorbed Secondary Antibody, Alexa Fluor Plus 594 (goat polyclonal, Thermo, A32740, 1:1000). Nuclei were counterstained with DAPI (Biosharp, 1:1000). Images were captured using a Leica DMI6000B microscopic imaging system. Images were analyzed with Image J software.

2.17. In vitro TNF-α stimulation assay

Mouse fibroblasts derived iAECs, human fibroblasts derived hiVECs, MAEC, HUVEC and HAVEC were exposed to 10 ng/mL TNF-α of the corresponding species for 4 h. Then the cells were fixed with 4 % paraformaldehyde and subjected to immunofluorescence using standard protocols and the following primary antibodies: anti-CD62E (E-selectin) (Rabbit monoclonal, Abcam, ab18981, 1:200), anti-CD62P (P-selectin) (mouse monoclonal, Abcam, ab6632, 1:200). Goat anti-Rabbit IgG (H + L) Highly Cross-Adsorbed Secondary Antibody, Alexa Fluor Plus 594 (goat polyclonal, Thermo, A32740, 1:1000) and Goat anti-Mouse IgG (H + L) Highly Cross-Adsorbed Secondary Antibody, Alexa Fluor Plus 488 (goat polyclonal, Thermo, A32723, 1:1000) specific to the appropriate species was used to detect bound primary antibodies. Nuclei were counterstained with DAPI (Biosharp, 1:1000). Images were captured using a Leica DMI6000B microscopic imaging system. Images were managed and analyzed by Image J software.

2.18. Alkaline phosphatase

Using Alkaline Phosphatase Stain Kit (Kaplow's/Azo Coupling Method) (Solarbio, G1480), alkaline phosphatase activity of the iPSCs was determined following manufacturer's protocol, images were visualized by DMI6000B Leica microscopic imaging system and analyzed using imaging analysis software (Image J).

2.19. Chromatin IP

ChIP assays were conducted using a commercial kit from Cell Signaling (#56383). Cells were seeded onto fibronectin coated PDMS of

different stiffnesses (each condition of ~2 × 10^7 cells). After treatments washing twice with ice cold PBS, cells were scraped into cold PBS with protease inhibitor cocktail (PIC), pelleted with centrifuge, and treated with 1 mL of ice-cold ChIP sonication cell lysis buffer plus PIC twice, 10 min each. Cells were further treated with 1 mL of ice-cold ChIP sonication nuclear lysis buffer for 20 min and sonicated with SONIC Vibra-Cell for 10 s (peak power, 130W, 20K Hz), and three cycles. For each IP, 100 μl of chromatin (~7 μg, DNA concentration determined by Nanodrop) was diluted into 400 μl of 1 × ChIP buffer with PIC. Ten microliters of sample of the diluted chromatin were chosen as the 2 % input sample. 2 μg H3K9me3 antibody (Cell Signaling, #13969), H3K27me3 antibody (Cell signaling, #9733), H3K4me3 antibody (Cell signaling, #9751) or RNA Pol II S2p antibody (Abcam, ab193468) were added to each diluted chromatin solution. Normal rabbit IgG antibody (2 μg, Cell Signaling, #56383) was used as the negative control. The IP samples were incubated at 4 °C overnight with rotation. Protein G magnetic beads (30 μl) were added to each IP reaction and incubated for 2 h at 4 °C with rotation. Protein G magnetic beads in each IP were pelleted by placing the tubes in a magnetic separation rack and washed with low-salt solution three times and high-salt solution once (5 min each at 4 °C with rotation). Chromatin was eluted from the antibody/protein G magnetic beads for 30 min at 65 °C with gentle vortexing (1200 rpm) by using a thermomixer from Eppendorf. Reverse cross-links were achieved by adding 6 μl of 5 M NaCl and 2 μl of proteinase K with incubation for 2 h at 65 °C. DNA was purified by using spin columns.

For ChIP-qPCR experiments, qPCR was conducted using SYBR Green Real time PCR Master Mix (TOYOBO, QPK-201) on CFX Connect Real-Time PCR Detection System (Bio-Rad). qPCR primers were designed and manufactured by TsingKe. The primer sequences are listed below as follows: mouse CD144 promoter primer set, CCACTAAGCCTC TGCTTTCTGA (forward) and CTGCCTGGGGTATTCAACTCAT (reverse); mouse CD31 promoter primer set, TCCTTTGGTGACTAAGCCGGT (forward) and AGACCTGTTTGCCTTTCCTGTG (reverse); mouse Flk1 promoter primer set, TTTGGTCCCTTGGGACTTTCAG (forward) and ATGTAGCCAGTAATGGGCTCTG (reverse); human CD144 promoter primer set, AGCCAGCCCAGCCCTCAC (forward) and CCTGTCAGCC-GACCGTCTTTG (reverse); Human CD31 promoter primer set, CGAGA-CAGAGGGAGGGTCAA (forward) and GGCCTGATATCTCCTCAGGAA (reverse); Human Flk1 promoter primer set, AGTAACAGGTTACATTA-TATTTCAG (forward) and GTACTCGGTAACGGGCGCTGAGCAAC (reverse).

2.20. Bulk RNA-sequencing

RNA-sequence data collection was performed following the published method [40]. M-20, human adult primary dermal fibroblast HDF, hiVECs (M-20-derived) on day 20, HDF-hiVECs (HDF-derived) on day 20, HUVECs, human primary aortic valve endothelial cells (HAVEC) were seeded in duplicates into 10 cm dishes and cultured until 80 % confluence was reached. After that, total RNA was harvested and isolated using the RNeasy Micro Kit (Qiagen, 74004). DNA digestion was performed using the RNase-Free DNase set (Qiagen, 79254). RNA quality was checked using Qubit and LabChip Touch (the same function as tapestation) (Table S3). RNA-seq reads from samples were aligned with STAR (v.2.5.2) using the default parameters to the Homo sapiens reference genome. SAM files were converted to BAM and sorted using Samtools (v.1.9). Count matrices were generated using the HTseq-count. Gene-wise differential expression in the sample dataset between distinct groups was performed using the R package DESeq2 (v.1.30.1). Normalized values for plots were obtained using the log function of the same package. Signature scores were defined as the scaled mean of all genes in the signature after scaling the expression matrix. Principal Component Analysis (PCA) values were generated with the Python's sklearn library using all genes expression value and visualized with R package ggplot2. The quality control of sample sequencing data was shown in Tables S3 and S4.

2.21. Construction of tissue engineered aortic valves

Hearts of adult pigs (weights ranging from 130 to 150 kg per pig) were obtained from a local abattoir. The hearts were then transferred to the laboratory in cold isotonic saline and immediately processed. Within 1 h of death, aortic valve leaflets were precisely dissected from the aortic root and rinsed with cold isotonic saline under aseptic conditions. Decellularized porcine aortic valves were prepared according to a previously reported method [41]. Then the decellularized valves were crosslinked by PGG to enhance mechanical properties [42]. At this time, the valves were called PGG-crosslinked decellularized aortic valves (PGG-DAV or simply DAV). iAECs or hiVECs were seeded onto PGG-DAV to co-culture for several days. On day 1, 4, 7, or 10, DiI-Ac-LDL, Calcein-AM and Hoechst 33258 were added to the cells on the heart valve for 4 h; NIH/3T3, M − 20, HDF cells were used as negative control; MAECs, HUVECs and HAVECs were used as positive control. Images were captured by three-dimensional reconstruction model using a Leica SP8 confocal microscopic imaging system. Images processing was via the Leica X software and images were analyzed by Image J. The success rate of this protocol was ~88 % for all experiments on decellularized porcine valves and the unsuccessful ones were due to poorly crosslinked porcine valves.

2.22. Bioreactor

5.0 x 10^5 iAEC PDMS 10 cells, MAECs, purified hiVECs, purified M-20-iPSC-hiVECs, purified PGP1-hiVECs and HUVECs were seeded on 5 mm × 7 mm PGG-DAV and cultured for 48 h. Then valves were cultured under flow for 5 days using a modified ibidi flow pump system of the bioreactor (Ibidi-10902, Germany). Flow parameters settings: Pressure, 67.7 mbar (1 mbar = 100 Pa); Shear stress, 10 dyn/cm^2; Flow rate, 4.29 ml min^{-1}; Shear rate, 149 s^{-1}. The medium in this system was replaced every other day. Under these conditions, the unidirectional laminar flow was provided to the cells. After the cells were sheared for defined duration under the fluid flow conditioning, cells were then fixed by 4 % paraformaldehyde. H&E staining and Masson's trichrome staining were performed and paraffin sections were labelled by CD31 and CD144 antibodies. This protocol was repeated at a rate of 75 % for all experiments in the bioreactor and the rest was due to poor adhesion of the cells on PGG-DHVs.

2.23. Abdominal aortic transplantation model

Immune deficient rats (nude rats) were purchased from Charles River. They were 6-weeks old male rats. Rats were grouped into PGG-DAV (No cells), murine iAEC PDMS 10-PGG-DAV (seeded with murine iAEC PDMS 10 cells), purified hiVEC-PGG-DAV (seeded with purified hiVECs), purified M-20-iPSC-hiVEC-PGG-DAV (seeded with purified M-20-iPSC-hiVECs), purified PGP1-hiVEC-PGG-DAV (seeded with purified PGP1-hiVECs), MAEC-PGG-DAV (seeded with MAECs), HUVEC-PGG-DAV (seeded with HUVECs). The cells seeded on the PGG-DHVs were frizzled into a tubular shape after they were washed with sterilized PBS 5 times to remove the detached and loosely adhered cells and xenomolecules before transplantation. Then the remaining cells on the PGG-DHVs were transplanted to the abdominal aorta of a nude rat. One or two months later, the valves were fixed by 4 % paraformaldehyde, H&E staining and Masson's trichrome staining were performed and paraffin sections were labelled by CD31, CD144, P-selectin (CD62P), E-selectin (CD62E), Collagen I (Abcam, ab88147, 1:200), Collagen III (Abcam, ab7778, 1:200), MMP13 (Abcam, ab39012, 1:200), MMP9 (Abcam, ab283575, 1:200), VEGFR2 (Cell signaling, #2479, 1:200), α-SMA (Abcam, ab119952, 1:500), NFATC1 (Thermo, #PA5-79730, 1:500), RUNX2 (Abcam, ab236639, 1:500), CD3 (Abcam, ab16669, 1:150) and CD68 (Abcam, ab283654, 1:100) antibodies. Analyzing all transplanted nude rats revealed that this protocol had a success rate of ~60 % because some nude rats died during surgical operation (these

were extremely difficult surgical procedures due to the small size of the rat abdominal aortic arteries).

2.24. Doppler ultrasonography

One month later, six nude rats in each group were selected to perform Doppler ultrasonography before they were sacrificed. Ultrasonic probe was put on the surface of abdomen at the site of operation; the probe was moved slowly and gently until a sharp image was obtained. The images would determine if the blood flow was unobstructed or not at the implant site of the valve. The red parts indicated that blood flow direction was toward the ultrasonic probe and the blue parts away from ultrasonic probe. Gradations of colors represented different blood flow rates according to the scale bar at the top left corner of each image. The oscillograms show the values of blood flow near the implant sites: waveform heights indicated the expected blood flow rates and the interval between the waveforms represented the heart rates of nude rats.

2.25. Evans blue staining

One month after iAECs or hiVECs graft transplantation, the nude rats were anesthetized by respiratory anesthesia machine and 3 % Evans blue (MCE, HY-B1102) solution (1 mL per kg body weight) was injected through the tail vein. After 30 min, the blood was drained. The muscle and adipose tissue around the transplanted site of abdominal aortic were collected up to 100 mg. 3 mL dimethylformamide (Aladdin, D171445) was added and placed at 50 °C for 24 h. The extract was centrifuged at 4000 rpm per min for 5 min and the supernatant was collected to measure the OD value at 620 nm. The concentration of Evans blue was calculated according to the protocol of specification.

2.26. Coagulation and anticoagulation function tests

One month after iAECs or hiVECs graft transplantation, the nude rats were anesthetized by respiratory anesthesia machine. The abdominal cavity was opened and the abdominal aorta was isolated. Blood was extracted with a syringe for coagulation function evaluated by automatic coagulation analyzer (Jiangsu Horner Medical Instrument Co., Ltd, H1204), including prothrombin time, thrombin time, activated partial thromboplastin time and fibrinogen concentration. Anticoagulation function tests, like antithrombin III concentration, were performed, according to the standard operating procedure of ELISA kit (Abcam, ab108801) to calculate the content of relevant indexes.

2.27. ELISA

The NIH/3T3, iAEC-PGG-DHV, MAEC, M-20, HDF, hiVEC-PGG-DHV, HDF-hiVEC-PGG-DHV, HUVEC and HAVEC cells were prepared, the purified Weibel-Palade body enriched fraction was obtained according to published paper [43]. Weibel-Palade body associated vWF and P-selectin were tested following the procedures in Human Von Willebrand Factor ELISA Kit (Abcam, ab108918), Human P-Selectin (CD62P) ELISA Kit (Abcam, ab272202), Mouse P-Selectin ELISA Kit (CD62P) (Abcam, ab200014); Mouse Von Willebrand Factor ELISA Kit (Abcam, ab314372). The absorbance at 450 nm was read in a microplate reader. All assays were done with triplicate samples.

2.28. Statistical analysis

Data was analyzed using GraphPad Prism Software. Differences between groups were calculated by independent Student's t-test plus Bonferroni correction (only two data groups compared) and multiple comparison of parametric analysis of variance (ANOVA) (more than two data groups) with recommended post-hoc corrections and Fisher's exact test when appropriate was used for statistics.

3. Results

3.1. Substrate stiffness regulates transdifferentiation efficiency

We explored a transdifferentiation strategy to induce the mouse embryonic fibroblasts (NIH/3T3 cell line) into aortic endothelial cell (AEC)-like cells or induced AECs (iAECs) *in vitro* (Fig. S1A). To achieve this goal, we established a protocol of adding various soluble chemicals and growth factors after different days (day 0 through day 11) of cell seeding on the rigid plastic dishes. This protocol was established after numerous trying and testing various regimens and modified from protocols from previously published reports [23–30,44–48]. The mechanisms of each factor used in our study to induce reprogramming of fibroblasts into endothelial cells have been published extensively in previous studies: azacytidine is a methyltransferase inhibitor which induces DNA demethylation to decondense chromatin [44,45]. Azacytidine addition was adopted as the first step in our protocol to induce fibroblasts into a transient precursor state. The following procedures are modified from the published protocol [46]: CHIR99021 and BMP4 promote Wnt and BMP signaling pathway activation; VEGF and DAPT promote formation and expansion of endothelial cells; HGF and PIGF increase the formation efficiency. 8-Br-cAMP is an agonist of cyclic AMP-dependent protein kinase and it is used to increase the efficiency of endothelial transdifferentiation; SB413542 promotes the maturation of endothelial cells [47].

Compared with the untreated 3T3 cells and mouse aortic endothelial cells (MAECs; positive controls), these cells exhibited different shapes from the 3T3 fibroblast cells but showed similar shapes as MAECs (Figs. S1B and S1C). Next, we examined two proteins that were uniquely expressed in endothelial cells. About twenty percent of the treated cells were positive for both vascular endothelial-cadherin (CD144) and platelet endothelial cell adhesion molecule 1 (CD31) using either the qRT-PCR assay (Fig. S1D), the FACS assay (Figs. S1E and S1F), the immunofluorescence assay (Figs. S1G and S1H), and the Western blot assay (Figs. S1I and S1J), suggesting that these cells entered an endothelial cell-like stage. We call these cells "induced aortic endothelial cells" (iAECs). Because the transdifferentiation efficiency was only ~20 % using this protocol, we explored the strategy of varying substrate stiffness which is known to impact cell fate [49], by plating the 3T3 cells on flexible substrates of PDMS (polydimethylsiloxane) (Fig. 1A) while keeping the chemical protocols the same as in Fig. S1A. The substrates of PDMS modulated the transdifferentiation efficiency and it appeared that PDMS 10 (Young's modulus of ~2.1 MPa, similar to the modulus of native aortic valves [50], but ~3 orders of magnitude lower than that of the ~2 GPa plastic dishes) was optimal, generating ~70 % $CD144^{+}CD31^{+}$ cells, either using the FACS assay (Fig. 1B and C) or the immunofluorescence assay (Fig. 1D and E). These iAECs on the PDMS 10 substrate also exhibited similar cell shapes as the MAECs (Fig. S1B) whereas 3T3 cells plated on the PDMS 10 substrate without the soluble chemicals maintained fibroblast-like cell shapes (Fig. S1B). To further improve the cell purity and to have complete transdifferentiation, the iAECs on day 11 were re-seeded without prior sorting/enrichment on PGG-crosslinked decellularized porcine heart valves for 10 additional days and incubated in specific induction medium. The re-seeding and subsequent culture appeared to have enriched for ECs and depleted non-ECs: on day 21, about 97 % of these cells were $CD144^{+}CD31^{+}$ cells, assayed either using the FACS (Fig. 1F and G) or immunofluorescence (Fig. 1H and I). Compared with those genes in 3T3 cells, iAECs on PGG-DHV on day 21 expressed *Flk1, CD31,* and *CD144*, almost reaching the levels of the positive controls-MAECs (Fig. S2A). In addition, fibroblast-associated genes *Vimentin*, *α-SMA (alpha-smooth muscle actin)*, and *S100a4* were not expressed in these iAEC-PGG-DHV cells and MAECs (Fig. S2B). Other endothelial cell markers, *Sox18, Sox17, Fli1, Elk3* and *Erg* were expressed in iAEC-PGG-DHV cells but they were lower than the levels of the positive control-MAECs, except for *Sox17,* which was at a similar level as MAECs (Fig. S2C). Together these results show

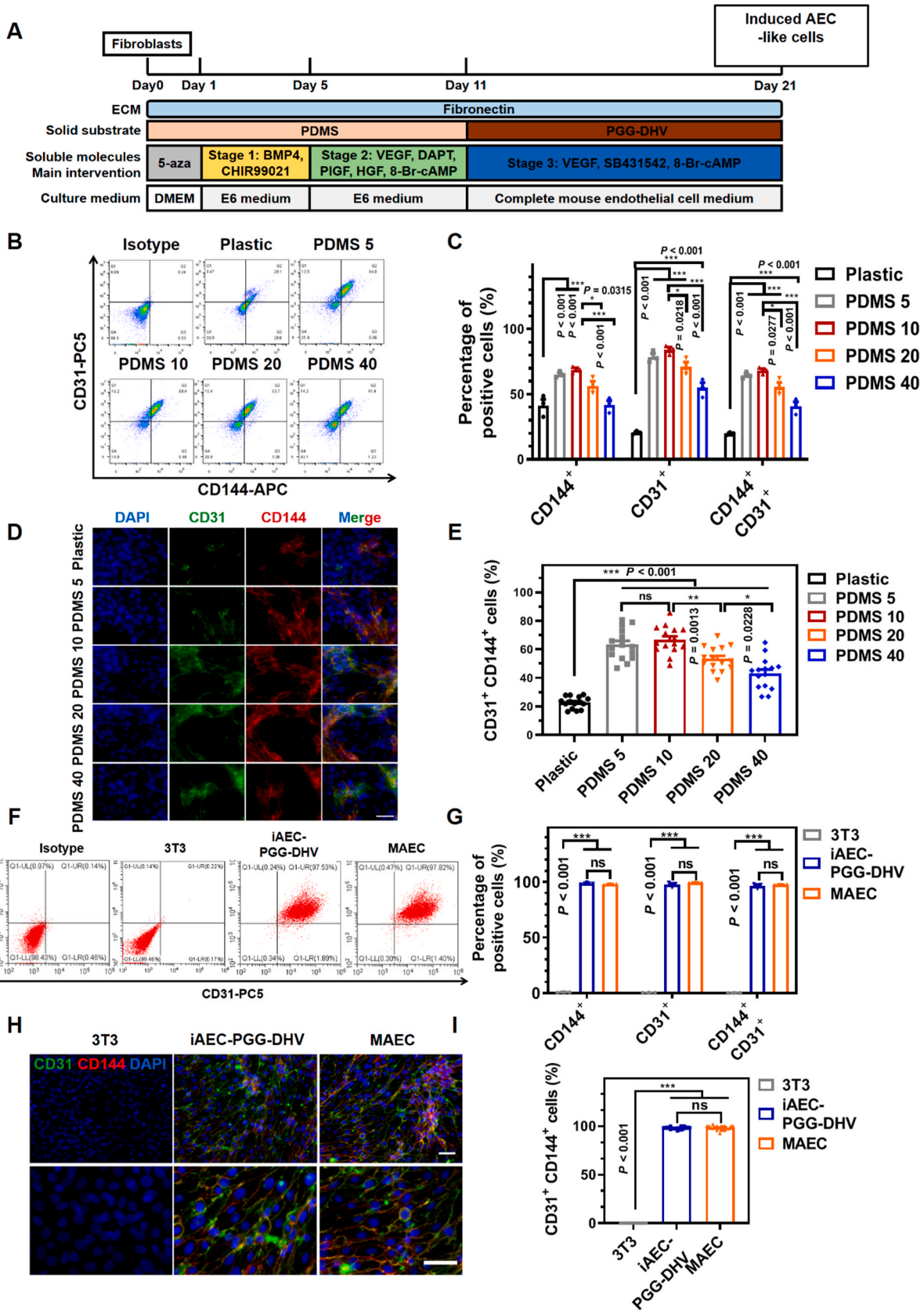

(caption on next page)

Fig. 1. Substrate stiffness regulates transdifferentiation efficiency of mouse fibroblasts to iAECs. (A) Mouse fibroblasts NIH/3T3 were seeded on Fibronectin-coated flat PDMS. Firstly, cells were treated with 5-azacytidine for 24h. Then, medium was changed to E6 medium containing BMP4 and CHIR99021. On day 5, medium was changed to E6 medium containing VEGF, DAPT, PIGF, HGF, 8-Br-cAMP. On day 11, iAECs were resuspended and seeded on PGG-crosslinked decellularized porcine heart valves for 10 days, medium changed to complete mouse endothelial cell medium containing VEGF, SB431542, 8-Br-cAMP. (B) Representative images of FACS quantification of CD31 and CD144 expression of iAEC- Plastic, iAEC- PDMS 5, iAEC- PDMS 10, iAEC- PDMS 20, iAEC- PDMS 40 on day 11. Each ratio of PDMS indicates the ratio of the base to curing agent, the stiffness of 5:1, 10:1, 20:1, 40:1 is 2.6, 2.1, 1.0, 0.1 MPa. (C) Histogram shows the quantification of FACS data from (B), mean ± s.e.m.; n = 3 separate experiments. (D) Representative images of immunofluorescence of CD31 and CD144 expression of iAEC- Plastic, iAEC- PDMS 5, iAEC- PDMS 10, iAEC- PDMS 20, iAEC- PDMS 40. Scale bar, 100 μm. (E) Quantification of $CD31^+$ $CD144^+$ positive cells from immunofluorescence data in (D), mean ± s.e.m.; n = 15 random viewfields in 3 dishes. (F) FACS analysis of CD31 and CD144 expression of iAEC seeded on PGG-DHV on day 21. (G) Quantification of FACS data in (F); Mean ± s.e.m.; n = 3 separate experiments. (H) Representative images of FACS quantification of CD31 and CD144 expression of iAEC seeded on PGG-DHV on day 21. Top panel, 20x; Bottom panel; 63x. Scale bar, 50 μm. (I) Quantification of immunofluorescence data in (H). Student's t-test plus Bonferroni correction (only two data groups compared) and multiple comparisons of parametric analysis of variance (ANOVA) (more than two data groups) with recommended post-hoc corrections when appropriate were used for statistics. *P < 0.05, **P < 0.01, ***P < 0.001, ns = not significantly different.

that combining inducing chemicals/growth factors with substrate stiffness manipulation provides an efficient way to transdifferentiate mouse fibroblasts into iAECs.

3.2. Mouse iAECs show similar functions as MAECs

To further examine if these iAECs were functional, we measured DiI-Ac-LDL uptake [51], tube formation capability, phosphorylation levels of VEGFR2 (vascular endothelial growth factor receptor 2), and levels of E-selectin and P-selectin in these cells. Cells with AEC-like functions express the scavenger receptors and DiI-labelled acetylate low-density lipoprotein (DiI-Ac-LDL) bind to scavenger receptors [52]. Like MAECs, mouse iAECs on pentagalloylglucose (PGG)-crosslinked decellularized porcine aortic valves (PGG-DAV or simply DAV) took up DiI-Ac-LDL, but 3T3 cells did not have any uptakes (Fig. 2A–D). The tube formation assay on Matrigel is a useful assay to assess if the cells behave like endothelial cells [48], and iAECs form capillary-like tubes in collagen gels [53]. iAECs formed numerous tube-like structures and lumens that could be perfused through by red blood cells, like those by MAECs, but 3T3 cells did not form any tubes and lumens (Fig. 2E and F and S3). Furthermore, the $CD31^-CD144^-$ cells isolated from the pool of iAECs did not take up DiI-Ac-LDL or form any tubes, the cell shape of $CD31^-CD144^-$ cells was similar with negative control 3T3 cells, which was consistent with published papers (Fig. S3) [54,55]. The VEGF (vascular endothelial growth factor) stimulation assay and TNF-α stimulation assay were two important methods to detect the activation potential of endothelial cells. Mouse iAECs seeded on PGG-DHV increased the phosphorylation level of VEGFR2, like MAEC, when treated with VEGF (Fig. 2G and H). Mouse iAECs seeded on PGG-DHV also increased the expression of E-selectin and P-selectin like MAEC when treated with TNF-α (Fig. 2I and J). Mouse iAECs seeded on PGG-DHV also increased the expression of Sox17 and Fli1 at the cell-cell junctions, the cytoplasm, and the nucleus, like MAEC (Fig. S4), and demonstrated the presence of P-selectin and vWF (Von Willebrand factor) within the Weibel Palade bodies of iAECs (Fig. S4). Importantly, seeding the cells on PGG-DAVs, iAEC PDMS 10 cells formed a confluent and intact endothelial cell layer on the surface of DAV on day 10 (Fig. 2A). During the transdifferentiation process, the cells did not express any pluripotency markers (Fig. S5), suggesting that the potential of tumor formation may not be an issue for these transdifferentiated cells.

3.3. Substrate stiffness regulates transdifferentiation via modulating H3K9me3

It is known that histone 3 at lysine 9 trimethylation (H3K9me3) is an important mark for gene suppression and demethylation of H3K9me3 is necessary for force-induced gene upregulation [56,57]. The expression tendency of H3K4me3 was opposite of H3K9me3, consistent with the notion that H3K9me3 and H3K27me3 are involved in chromatin condensation but H3K4me4 is associated with chromatin decondensation [58]. To examine whether substrate stiffness regulates transdifferentiation via altering H3K9me3, we assayed H3K9me3 in cells under various substrate stiffness. Using western blotting assay, immunofluorescence assay, and FACS assay, we found that the level of H3K9me3 was lowest in iAEC PDMS 10 cells (Figs. S6A–D). In addition, the chromatin immunoprecipitation (ChIP) assay revealed that H3K9me3 levels were lowest at the promoter sites of *Flk1, CD31,* and *CD144* in iAEC PDMS 10 and PDMS 5 cells (Fig. S6E). These results were supported by the data that RNA Pol II S2p levels were highest at the promoter sites of *Flk1, CD31,* and *CD144* in iAEC PDMS 10 cells (Fig. S6F). To examine the effect of individual soluble molecules in transdifferentiation, we removed them one by one at various stages. Removing any of those 7 soluble molecules decreased the percentage of $CD31^+CD144^+$ cells but removing VEGF resulted in the most down-regulation effect as it decreased the $CD31^+CD144^+$ cells from ~60 % to a few percent (Figs. S6G and S6H). Furthermore, during stage 2 (day 6 through day 11 of the whole protocol), mouse $CD31^+CD144^+$ cells only started to show up at day 2 of stage 2 (day 7 of the protocol) and they reached a maximum percentage on day 6 of stage 2 (day 11 of the protocol) (Figs. S6I and J). The percentage of H3K27me3 positive cells was also the lowest on PDMS 10 substrates, like that of H3K9me3 (compare Figs. S7A and B with S7C & D); in contrast, the percentage of H3K4me3 positive cells was the highest on PDMS 10 substrates (Figs. S7F and S7G), opposite those trends of H3K9me3 and H3K27me3. However, there was no significant difference in H3K27me3 and H3K4me3 levels at the promoter sites of *Flk1, CD31,* and *CD144* among various substrate stiffnesses (Figs. S7E and S7H). These results suggest that when the substrate stiffness matches that of the aortic valve *in vivo*, gene suppression by H3K9me3 is abrogated such that the transdifferentiation process becomes efficient and this process is not dependent on H3K27me3 or H3K4me3. These results suggest that all 7 select soluble molecules in the assay are necessary in the transdifferentiation protocol. Together these findings suggest that our protocol of using a solid substrate whose modulus is like the native aortic valve and 7 select soluble molecules can induce an efficient transdifferentiation of mouse embryonic fibroblasts into iAECs.

One issue is whether the duration of transdifferentiation in our protocol is optimal. After the first 24-h treatment with 5-azacytidine, the gene suppression mark H3K9me3 already started to decrease on various substrate stiffness of fibronectin-coated PDMS and the cells on PDMS 10 (2.1 MPa stiffness, similar to native aortic valve stiffness) had the lowest H3K9me3 levels (Fig. S8) and Vimentin expression was also decreased (Figs. S9A and S9B) suggesting that the 24-h treatment with 5-azacytidine at the start of the protocol is important in facilitating gene expression and fibroblast reprogramming during transdifferentiation. Without 24-h treatment with 5-azacytidine, there would be no initiation of reprogramming; in contrast, keeping 5-azacytidine in the medium much longer than 24 h (e.g., for several days) would not continue the process of reprogramming. Vimentin expression decreased but Brachyury expression increased slightly on day 5 (Figs. S9A–D). Vimentin expression decreased further but Brachyury expression returned to pre-treatment levels on day 11 (Fig. S9). These results suggest the transdifferentiation protocol of 11 plus 10 (total 21) days of transdifferentiation is optimal under our culture conditions and longer

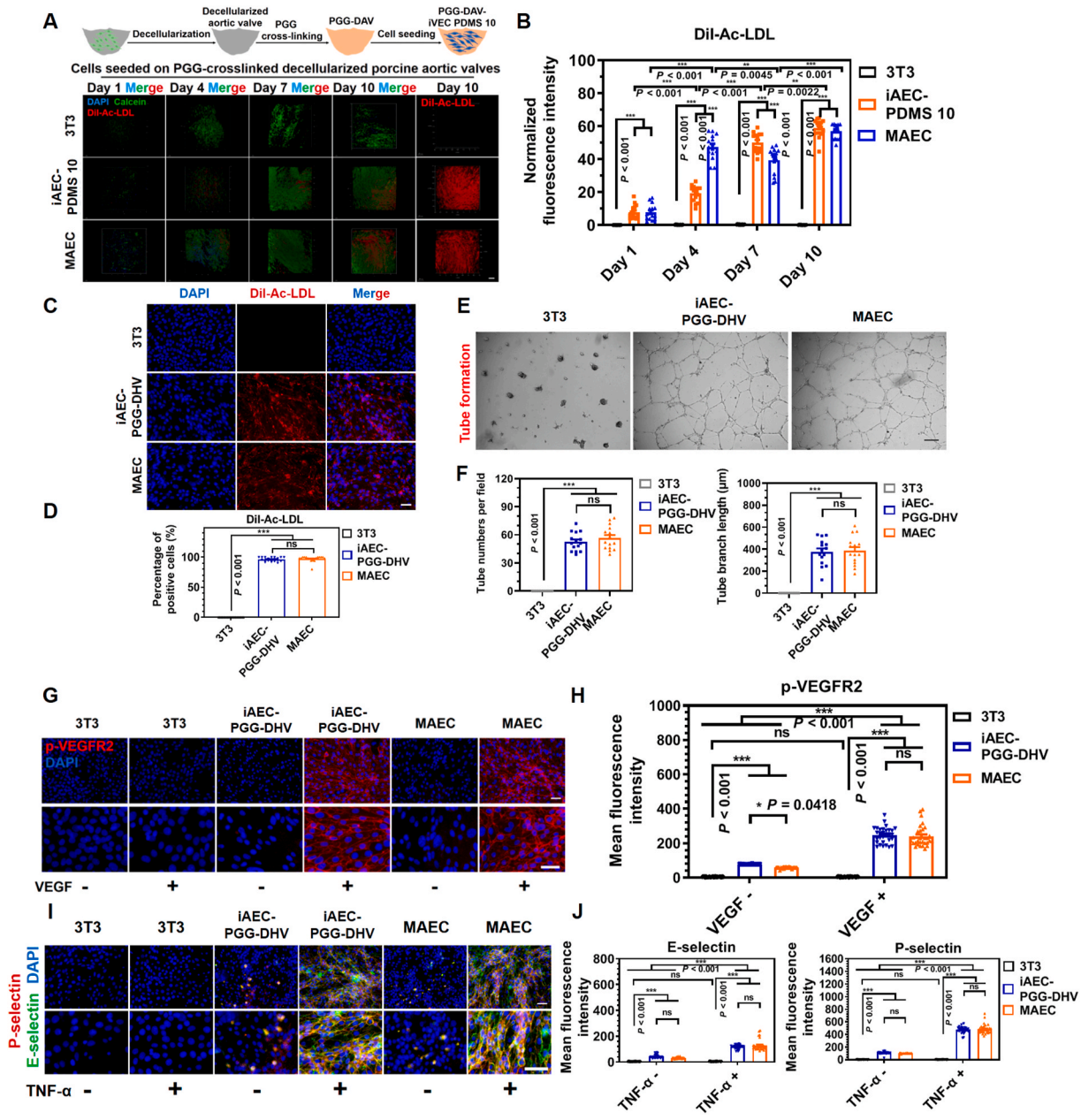

Fig. 2. iAECs show similar functions as MAECs. (A) Representative confocal fluorescence images of different cell types adhering on PGG-crosslinked decellularized porcine aortic valves (PGG-DAV) uptaking DiI-Ac-LDL (red color), Calcein-AM (green color) and Hoechst (blue color) on day 1, 4, 7 and 10. (B) Quantification of relative fluorescence intensity per μm^2 in each viewfield on day 1, 4, 7 and 10. Mean ± s.e.m.; n = 15 viewfields. (C) The level of DiI-Ac-LDL uptake in NIH/3T3, iAEC seeded on PGG-DHV on day 21 and positive control MAEC. (D) Quantification of DiI-Ac-LDL uptake in (C); Mean ± s.e.m.; n = 20 random viewfields in 3 dishes. Scale bar, 50 μm. (E) The representative images of tube formation of NIH/3T3, iAEC seeded on PGG-DHV on day 21 and positive control MAEC (All cells were seeded on Matrigel for 24h); Scale bar, 200 μm. (F) Quantification of tube numbers and branch lengths in (E); Mean ± s.e.m.; n = 15 random viewfields in 3 dishes from 3 separate experiments. (G) Immunofluorescence of phosphorylation of VEGFR2 expression of NIH/3T3, iAEC seeded on PGG-DHV on day 21 and MAEC when treated with VEGF. Top panel, 20 × ; Bottom panel; 63 × .Scale bar, 50 μm. (H) Quantification of immunofluorescence data in (G). Mean ± s.e.m.; n = 30 random viewfields in 3 dishes. (I) Immunofluorescence of the expression of E-selectin and P-selectin in NIH/3T3, iAEC seeded on PGG-DHV on day 21 and MAEC when treated with TNF-α. Top panel, 20 × ; Bottom panel; 63 × .Scale bar, 50 μm. (J) Quantification of immunofluorescence data in (I). Mean ± s.e.m.; n = 30 random viewfields in 3 dishes. Student's t-test plus Bonferroni correction (only two data groups compared) and multiple comparisons of parametric analysis of variance (ANOVA) (more than two data groups) with recommended post-hoc corrections when appropriate was used for statistics. *P < 0.05, **P < 0.01, ***P < 0.001, ns = not significantly different.

durations are not necessary. Taken together, all these results suggest that mouse iAECs on day 21 exhibit AEC-like functions, have excellent biocompatibility on decellularized porcine heart valves, can proliferate, and maintain functions similarly as MAECs.

3.4. Transdifferentiation of human fibroblasts to hiVECs

Next, we transdifferentiated human embryonic fibroblasts M-20 cells into VEC-like cells using a modified protocol of adding growth factors after different days (day 0 through day 9) of cell seeding on the rigid plastic dishes coated with a thin layer (<1 μm) of Matrigels (Fig. S10A). This protocol was established after trying and testing various regimens

and modifying protocols from previous published reports [59,60]. Human embryonic fibroblast M-20 cells were seeded on Matrigel-coated plates. First, cells were treated with 5-azacytidine for 24h. Then, medium was changed to E6 or N2B27 medium containing BMP4 and Wnt3a. On day 2, medium was changed to E6 or N2B27 medium containing BMP4 and bFGF. On day 3, medium was changed to E6 or StemPro-34 medium containing VEGF and bFGF. On day 9, induced hiVECs were resuspended and sorted by MACS and were then seeded on rigid plastic coated with Matrigel to continue expanding. The medium was changed to human endothelial growth medium EGM-2 containing VEGF, SB431542, 8-Br-cAMP. On day 13, these cells were reseeded on PGG-crosslinked decellularized porcine heart valves for 7 days. After transdifferentiation via this protocol, these human embryonic fibroblast M-20 cells exhibited the classical cobblestone morphology when compared to the HUVECs (Figs. S10B and S10C). Because the M-20 cells were embryonic fibroblasts, they might be multipotent and were not an optimal source for transdifferentiation. As such, we transdifferentiated human adult primary dermal fibroblasts (HDFs) into hiVECs using a different protocol from the M-20 protocol by plating the HDFs on 2.1 MPa PDMS substrate for 13 days and then switching them to PGG-DAV (Fig. 3A). On day 13 before seeding the cells on the decellularized porcine aortic valve, ~10 % of the cells expressed are $CD144^{+}CD31^{+}$ on PDMS 10 (2.1 MPa) whereas for those on the rigid glass ~5 % of the cells are $CD144^{+}CD31^{+}$ (Fig. 3B and C). After MACS (magnetic-activated cell sorting) on day 13, the $CD144^{+}CD31^{+}$ cells increased to ~80 %, still lower than HUVECs (Fig. 3D and E). However, after plating the cells on the decellularized porcine aortic valve (PGG-DAV) for 7 additional days, on day 20 these human adult fibroblast cells exhibited the classical cobblestone morphology when compared to the HUVECs and the human primary aortic valvular endothelial cells (HAVECs), which was used as the "gold" standard cells for comparison (Fig. S10). The trans-differentiation protocols forced these human fibroblasts (M-20 and HDF) to express elevated levels of endothelial markers *Flk1, CD31, CD144, Sox18, Sox17, Fli1, Elk3,* and *Erg* but no fibroblast markers *Vimentin, α-SMA* and *S100a4*, just like HUVECs and HAVECs (Fig. 4A–C). About 95 % of the cells were $CD144^{+}CD31^{+}$ after they were sorted by MACS, quantified by FACS (Fig. 4D and E) or immunofluorescence (Fig. 4F and G), suggesting that they are highly pure VEC-like cells. The DEGs analysis of RNA-seq (Fig. 4H), specialized heatmap (Fig. 4I) and PCA analysis (Fig. 4J) show hiVECs were more like HAVECs than HUVECs. RNA-seq data show that no endothelial cells were contaminated in human fibroblasts(Fig. 4I and J). hiVECs, either from M-20 or from HDF, highly expressed 25 VEC-specific pan markers such as *NFATC1, C7, OIT3, IL1RL1, NNAT, GIMAP6, GJA4, MYCT1, CLEC1B, GIMAP4* and other markers, like HAVECs but drastically different from HUVECs (Fig. 4I). PCA analysis of RNA-seq results shows that HDF and M-20 cells belonged to the same population inside the red box; HDF and M-20-derived hiVECs belonged to the same population as the gold standard HAVECs inside the blue box, but not with HUVECs inside the green box (Fig. 4J). Together these results suggest that the hiVECs are transdifferentiated more similarly to the HAVECs than the HUVECs.

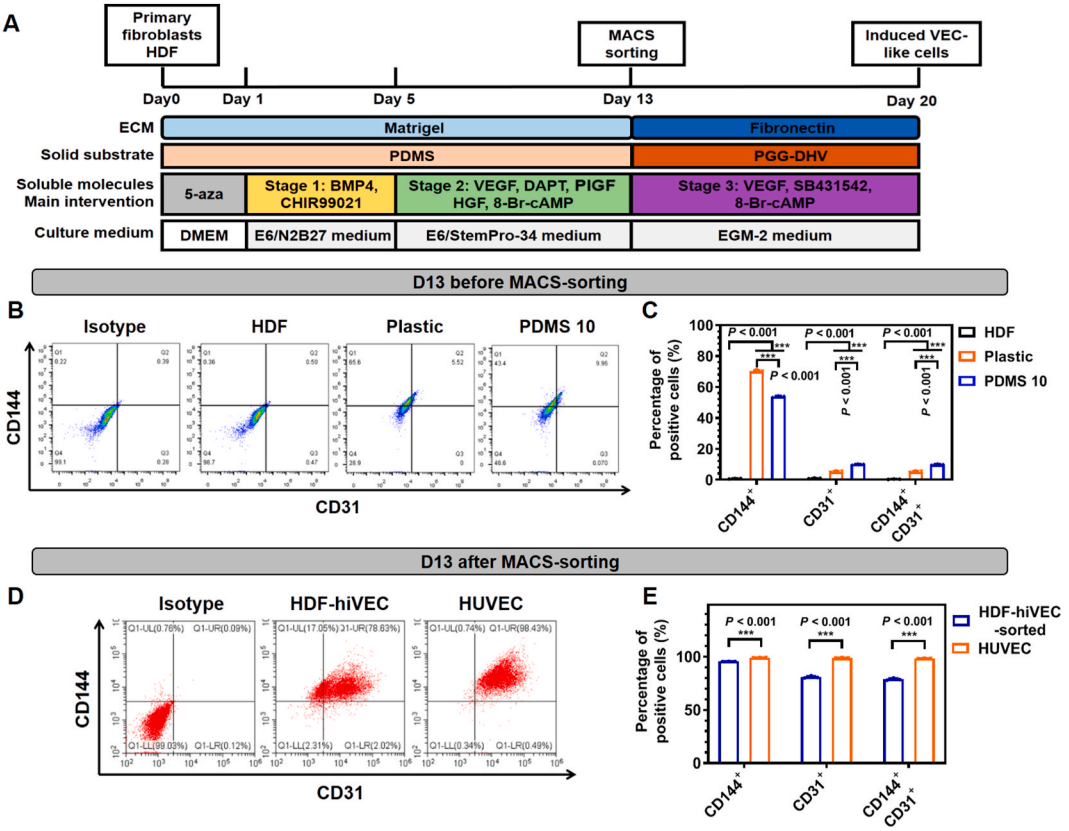

Fig. 3. Substrate stiffness regulates transdifferentiation efficiency of human adult primary dermal fibroblasts to hiVECs. (A) Human primary dermal fibroblasts (HDF) were seeded on Matrigel-coated flat PDMS. Firstly, cells were treated with 5-azacytidine for 24h. Then medium was changed to E6 medium or N2B27medium containing BMP4 and CHIR99021. On day 5, medium was changed to E6 medium or StemPro-34 medium containing VEGF, DAPT, PIGF, HGF, 8-Br-cAMP. On day 13, hiVECs were resuspended and enriched by MACS; they were seeded on PGG-crosslinked decellularized porcine heart valves for 7 days and medium changed to human endothelial growth medium EGM-2 containing VEGF, SB431542, 8-Br-cAMP. (B) Representative images of FACS quantification of CD31 and CD144 expression of hiVEC- Plastic, hiVEC- PDMS 10. Ratio of PDMS indicates the ratio of the base to curing agent, the stiffness of 10:1 is 2.1 MPa. (C) Histogram shows the quantification of FACS of (B), mean ± s.e.m.; n = 3 separate experiments. (D) FACS analysis of CD31 and CD144 expression of MACS sorted HDF-hiVEC. (E) Quantification of FACS data in (D); Mean ± s.e.m.; n = 3 separate experiments. Student's t-test plus Bonferroni correction or ANOVA was used; ***$P < 0.001$; ns = not significantly different.

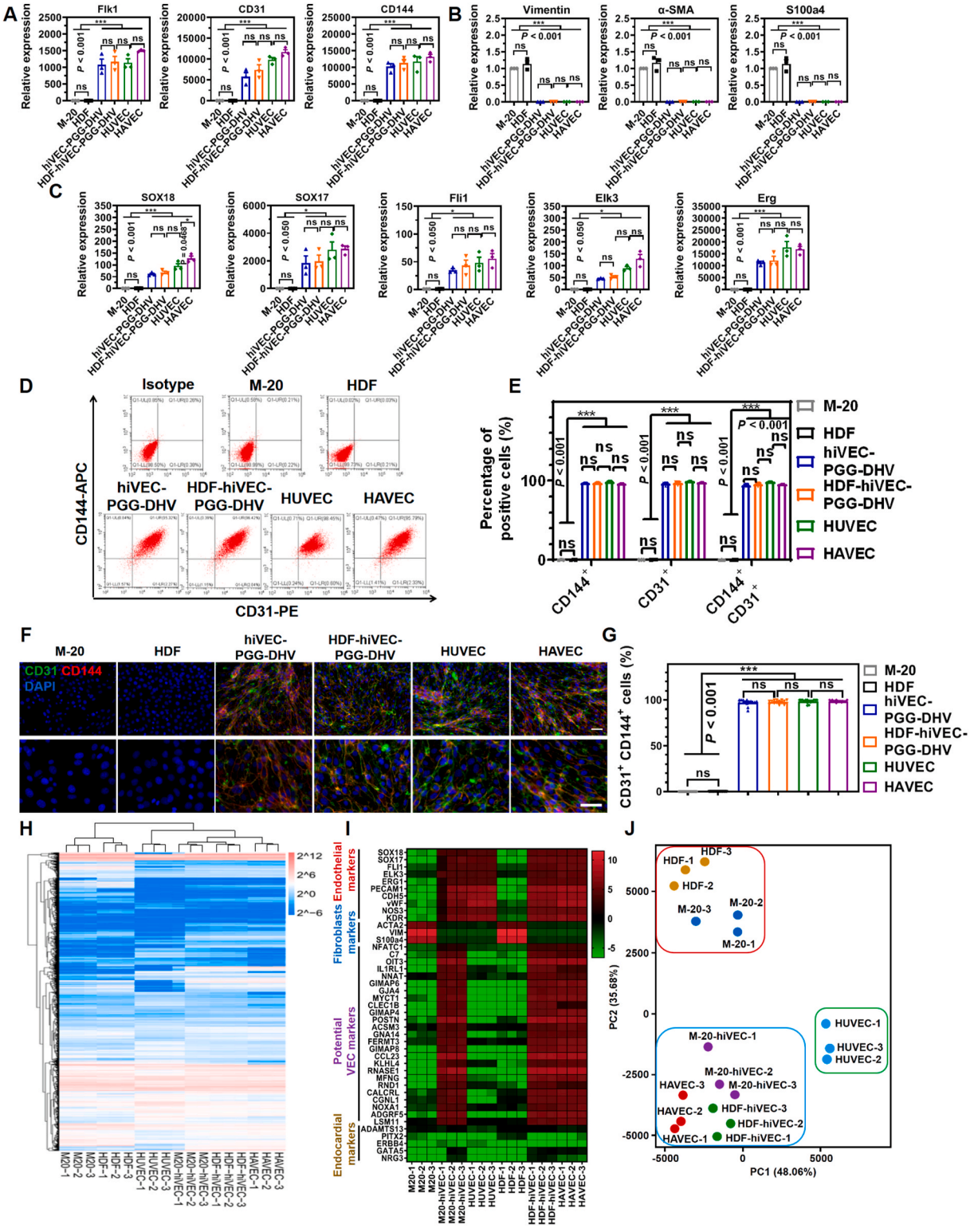

(caption on next page)

Fig. 4. Transdifferentiation of human fibroblasts to hiVECs. (A) Quantification of the expression of VEC-associated genes (Flk1, CD144 and CD31) of M-20, HDF (primary human dermal fibroblast), purified M-20-derived hiVEC seeded on PGG-DHV, purified HDF-derived hiVEC seeded on PGG-DHV for 7 days, HUVEC and HAVEC (primary human aortic valve endothelial cell). (B) Quantification of the expression of fibroblast-associated genes (Vimentin, α-SMA, S100a4) of M-20, HDF, purified M-20-derived hiVEC seeded on PGG-DHV, purified HDF-derived hiVEC seeded on PGG-DHV for 7 days, HUVEC and HAVEC. (C) Quantification of the expression of EC-associated genes (Sox18, Sox17, Fli1, Elk3 and Erg) of M-20, HDF, purified M-20-derived hiVEC seeded on PGG-DHV, purified HDF-derived hiVEC seeded on PGG-DHV for 7 days, HUVEC and HAVEC. Mean ± s.e.m.; n = 3 separate experiments. (D) FACS analysis of CD31 and CD144 expression of M-20, HDF, M-20 and HDF derived and MACS-enriched hiVEC seeded on PGG-DHV for 7 days, HUVEC and HAVEC. (E) Quantification of FACS data in (D); Mean ± s.e.m.; n = 3 separate experiments. (F) Representative images of immunofluorescence of CD31 and CD144 expression of M-20, HDF, M-20 and HDF derived MACS-sorted hiVEC seeded on PGG-DHV for 7 days, HUVEC and HAVEC. Top panel, 20 × ; Bottom panel; 63 × .Scale bar, 50 μm. (G) Quantification of $CD31^+$ $CD144^+$ positive cells in (F), mean ± s.e.m.; n = 15 random viewfields in 3 dishes. (H) Transcriptome comparison and unsupervised clustering between human fibroblasts, hiVECs, HUVEC and the HAVEC. All DEGs (60,000+ genes) analysis of the shared genes between human fibroblasts M20 and HDF, hiVECs, HDF-hiVECs, HUVEC and HAVEC. The numbers 1, 2, and 3 denote 3 independent experiments for each cell type. (I) Heatmap analysis showing the endothelial markers, fibroblasts markers, potential VEC markers, or endocardial markers expressed in human fibroblasts, hiVECs, HDF-hiVECs, HUVEC, or HAVEC. (J) PCA (Principal Component Analysis) of the shared genes between human fibroblasts, hiVECs, HDF-hiVECs, HUVECs, and HAVECs. Student's t-test plus Bonferroni correction (only two data groups compared) and multiple comparisons of parametric analysis of variance (ANOVA) (more than two data groups) with recommended post-hoc corrections when appropriate was used for statistics. $*P < 0.05$, $**P < 0.01$, $***P < 0.001$, ns = not significantly different.

3.5. Human hiVECs show similar functions as HAVECs

The purified hiVECs from M-20 cells and the purified HDF-hiVECs from HDF cells cultured on the porcine decellurized valves proliferated, became confluent, and covered the whole valve surface 7 days after culture (Fig. 5A and B). On separate experimental assays of the tube formation on Matrigel, hiVECs and HDF-hiVECs formed numerous tube-like structures and lumens which could be perfused through by red blood cells, similar to HUVECs and HAVECs; however, the non-transdifferentiated fibroblasts of M-20 and HDF cells could not form any tubes (Fig. 5C and D and S3). Like HUVECs and HAVECs, hiVECs and HDF-hiVECs took up DiI-Ac-LDL, but M-20 and HDF cells did not have any uptakes (Fig. 5E and F). Furthermore, the $CD31^-CD144^-$ cells isolated from the pool of VEC-like cells did not take up DiI-Ac-LDL and did not form any tubes (Fig. S11). hiVECs seeded on PGG-DHV increased phosphorylation levels of VEGFR2, like HUVECs and HAVECs when treated with VEGF (Fig. 5G and H). hiVECs and HDF-hiVECs seeded on PGG-DHV increased expressions of E-selectin and P-selectin, like HUVECs and HAVECs when treated with TNF-α (Fig. 5I and J). hiVECs seeded on PGG-DHV also increased the expression of Sox17 and Fli1 at both gene and protein levels; the proteins were distributed at the cell-cell junctions, the cytoplasm, and the nucleus, like HUVEC and HAVEC (Fig. 4C and S4C and S4D). Furthermore, P-selectin and vWF within the Weibel Palade bodies were present in hiVECs and HDF-hiVECs (Fig. S4). During the entire process of transdifferentiation, there was no expression of pluripotency markers OCT4 and Nanog (Fig. S12). To examine the effect of individual soluble molecules in transdifferentiation, we removed them one by one at various stages (stage 1 to stage 3). Removing any of those 4 soluble molecules decreased the percentage of $CD31^+CD144^+$ cells but removing VEGF had the most downregulation effect (Fig. S13). We also assessed how the duration of stage 3 impacted the transdifferentiation efficiency and found that the percentage of $CD31^+CD144^+$ cells reached the peak value on day 6 (Fig. S13). In addition, the chromatin immunoprecipitation (ChIP) assay revealed that H3K9me3 levels were lowest at the promoter sites of Flk1, CD31, and CD144 in hiVEC PDMS 10 cells (Fig. S14A), RNA Pol II S2p levels were highest at the promoter sites of Flk1, CD31, and CD144 in hiVEC PDMS 10 cells (Fig. S14D), but there was no significant difference in H3K4me3 and H3K27me3 levels at these promoter sites among various substrate stiffnesses (Figs. S14B and S14C). From the first 24 h treatment to stage 2 and then to stage 3, Vimentin expression continued to decrease while Brachyury increased slightly at stage 2 but returned to baseline levels on day 9 (Figs. S15A–D). These results suggest the protocol of human fibroblast transdifferentiation is optimal under our culture conditions and longer durations are not necessary. Together these results demonstrate that human fibroblasts-(such as M-20 or HDF) derived hiVECs are remarkably like human primary aortic valvular endothelial cells (HAVECs), as such, they may be called VEC-like cells.

3.6. iAECs and hiVECs stay functional on decellularized valves after fluid shear stress application

Cell seeding and attachment are the first two crucial steps that can lead to *in vitro* formation of tissue engineered aortic valves. To further determine how iAECs and hiVECs behave in an in-vivo like condition, bioreactors were used to mimic the real fluid shear stress environment in the vasculature. Mouse AEC-like cells (iAECs PDMS 10) or human VEC-like cells (purified hiVECs) were seeded on PGG-DAVs for 7–10 days and then were placed into the bioreactor to incubate for 5 days (Fig. 6A and S16A), hematoxylin and eosin (H&E) staining showed the engineered aortic valves exhibited a monolayer of cells adhered on the valve surface and Masson's trichrome stain showed collagen and elastic fibers and a distinct cell monolayer (Fig. 6B). Immunofluorescence assays showed prominent expressions of CD31 and CD144 in iAECs PDMS 10 or purified hiVECs (Fig. 6C–E). These results suggest that after 5-day fluid shear stress iAECs PDMS 10 and purified hiVECs attach firmly to the decellularized porcine aortic valves and exhibit VEC-like characteristics on the engineered aortic valves.

3.7. In vivo assessment of iAECs and hiVECs-based engineered aortic valves

To further examine how iAECs PDMS 10 or purified hiVECs seeded on the decellularized aortic valves would behave *in vivo*, we transplanted them to immune-compromised rats (nude rats). Because the rat aortic valves were too small to be operated on and to be replaced by the engineered aortic valves, we had to roll up the engineered aortic valve into a tube and grafted it at the abdominal aorta to simulate the dynamic *in-vivo* flow condition (Fig. 7A and S16B). Doppler ultrasonography was performed before rats were sacrificed 30 days after transplantation. The blood flow was not obstructed at the implant site of the engineered valve in all six rats of each set 30 days after valve graft transplantation (Fig. 7B; data from 5 additional sets of rats are shown in Fig. S16). Evans blue staining shows that none of the rats had vascular leakage after *in-vivo* transplantation (Fig. S17A); Coagulation and anticoagulation function tests show that all rats had normal coagulation and anti-coagulation functions and no thrombosis after *in-vivo* transplantation (Figs. S17B–F), consistent with Doppler ultrasonography data. H&E staining and Masson's trichrome staining show that 30 days after *in-vivo* transplantation all rats had intact engineered aortic valves with collagen or elastic fibers and the interior surface of the valvular tube exhibited a cell monolayer of iAECs or hiVECs in all rats except the no-cell control rats (Fig. 7C and D). In addition, compared with the positive control cells-MAECs and HUVECs, iAECs or hiVECs expressed similar levels of CD31 and CD144 whereas the no-cell control DAVs did not express any (Fig. 7E–G).

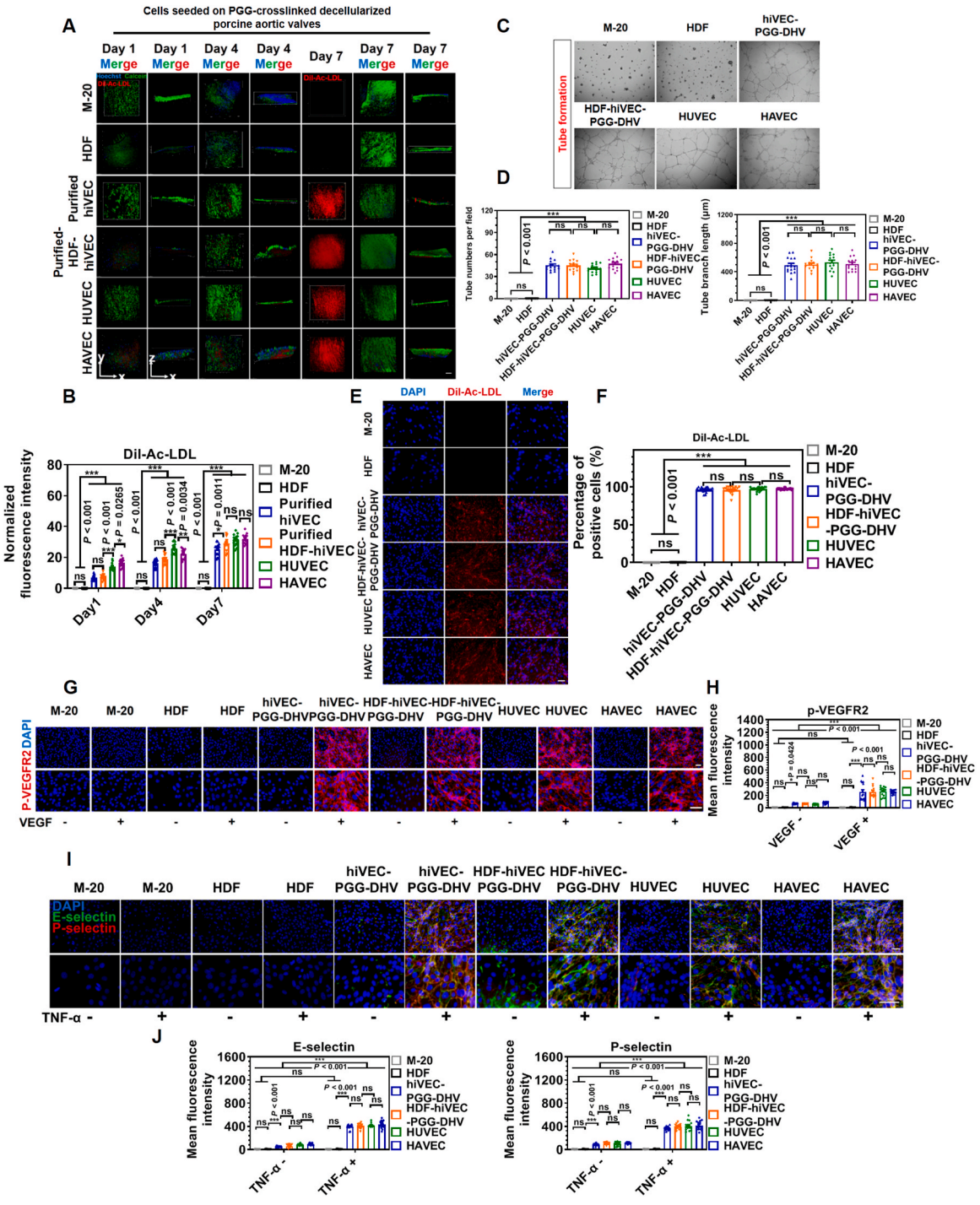

Fig. 5. Human induced VECs show similar functions as HUVECs and HAVECs. (A) Representative confocal fluorescence images of different cell types adhering on PGG-crosslinked decellularized porcine aortic valves (PGG-DAV) uptaking DiI-Ac-LDL (red color), Calcein-AM (green color) and Hoechst (blue color) on day 1, 4 and 7. (B) Quantification of relative fluorescence intensity per μm^2 in each viewfield on day 1, 4 and 7. Mean ± s.e.m.; n = 15 viewfields. (C) Representative images of tube formation of M-20, HDF, hiVEC and HDF-hiVEC seeded on PGG-DHV on day 20 and positive control HUVEC and HAVEC (All cells were seeded on Matrigel for 24h). Scale bar, 200 μm. (D) Quantification of tube numbers and branch lengths in (C); Mean ± s.e.m.; n = 15 random viewfields in 3 dishes. (E) The level of DiI-Ac-LDL uptake in M-20, HDF, hiVEC and HDF-hiVEC seeded on PGG-DHV on day 20 and positive control HUVEC and HAVEC. (F) Quantification of DiI-Ac-LDL uptake in (E); Mean ± s.e.m.; n = 20 random viewfields in 3 dishes. Scale bar, 50 μm. (G) Immunofluorescence of phosphorylation of VEGFR2 expression of M-20, HDF, hiVEC and HDF-hiVEC seeded on PGG-DHV on day 20 and positive control HUVEC and HAVEC when treated with VEGF. Top panel, 20 × ; Bottom panel; 63 × . Scale bar, 50 μm. (H) Quantification of immunofluorescence data in (G). Mean ± s.e.m.; n = 15 random viewfields in 3 dishes. (I) Immunofluorescence of the expression of E-selectin and P-selectin in M-20, HDF, hiVEC and HDF-hiVEC seeded on PGG-DHV on day 20 and positive control HUVEC and HAVEC when treated with TNF-α. Top panel, 20 × ; Bottom panel; 63 × . Scale bar, 50 μm. (J) Quantification of immunofluorescence data in (I). Mean ± s.e.m.; n = 15 random viewfields in 3 dishes. Student's t-test plus Bonferroni correction (only two data groups compared) and multiple comparisons of parametric analysis of variance (ANOVA) (more than two data groups) with recommended post-hoc corrections when appropriate were used for statistics. *$P < 0.05$, **$P < 0.01$, ***$P < 0.001$, ns = not significantly different.

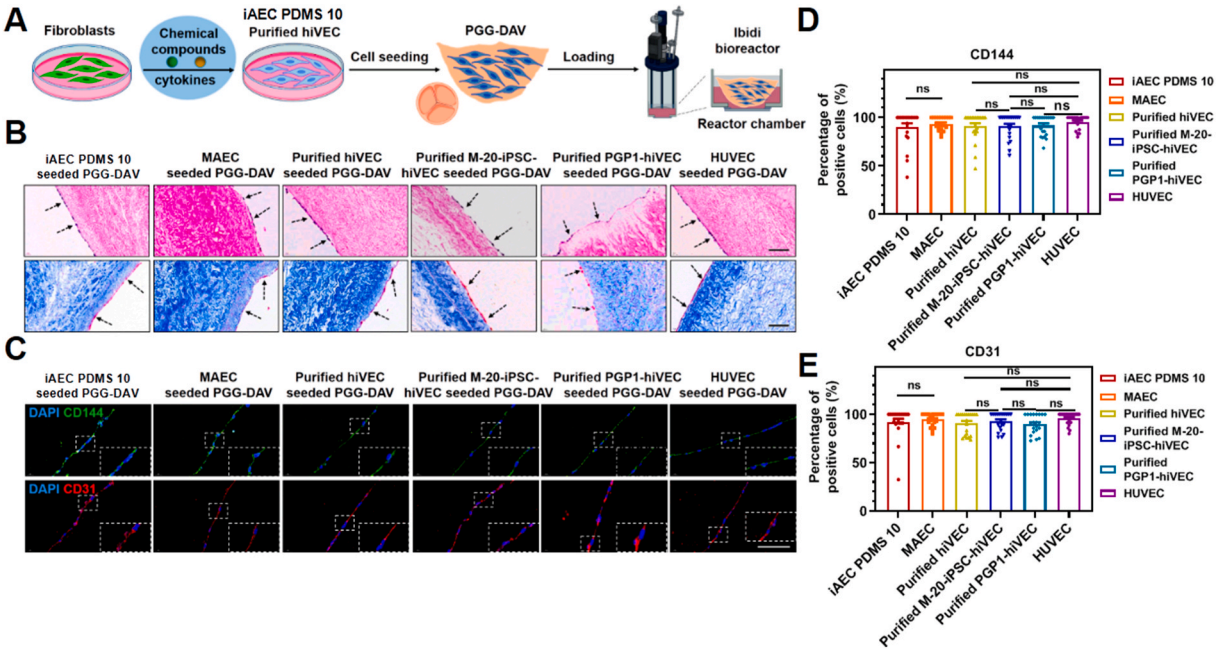

Fig. 6. iAECs and hiVECs stay functional on decellularized valves after fluid shear stress application. (A) Representative images of bioreactor experiments; Bioreactor experiment: iAEC PDMS 10, MAEC, Purified hiVEC, HUVEC cells were seeded on 7 mm × 5 mm PGG-crosslinked decellularized aortic valve pieces (PGG-DAV), cells were cultured in incubator for 48h. After that, heart valve pieces were installed in reaction cavities, culture medium was added. Priming the system, shearing force was set at 10 dyn/cm^2. Five days later, the heart valves were taken out and fixed in 4 % paraformaldehyde; Hematoxylin and eosin (H&E) staining, Masson's trichrome staining, and immunocytochemistry were performed. (B) Representative images of HE staining and Masson's trichrome staining. Scale bars, 50 μm. (C–E) Representative images and quantification of immunofluorescence of CD144, CD31; Scale bar, 50 μm; Mean ± s.e.m.; n = 21 random viewfields in 3 heart valve pieces. Student's t-test plus Bonferroni correction or ANOVA was used for statistics. $^*P < 0.05$, $^{**}P < 0.01$, $^{***}P < 0.001$; ns = not significantly different.

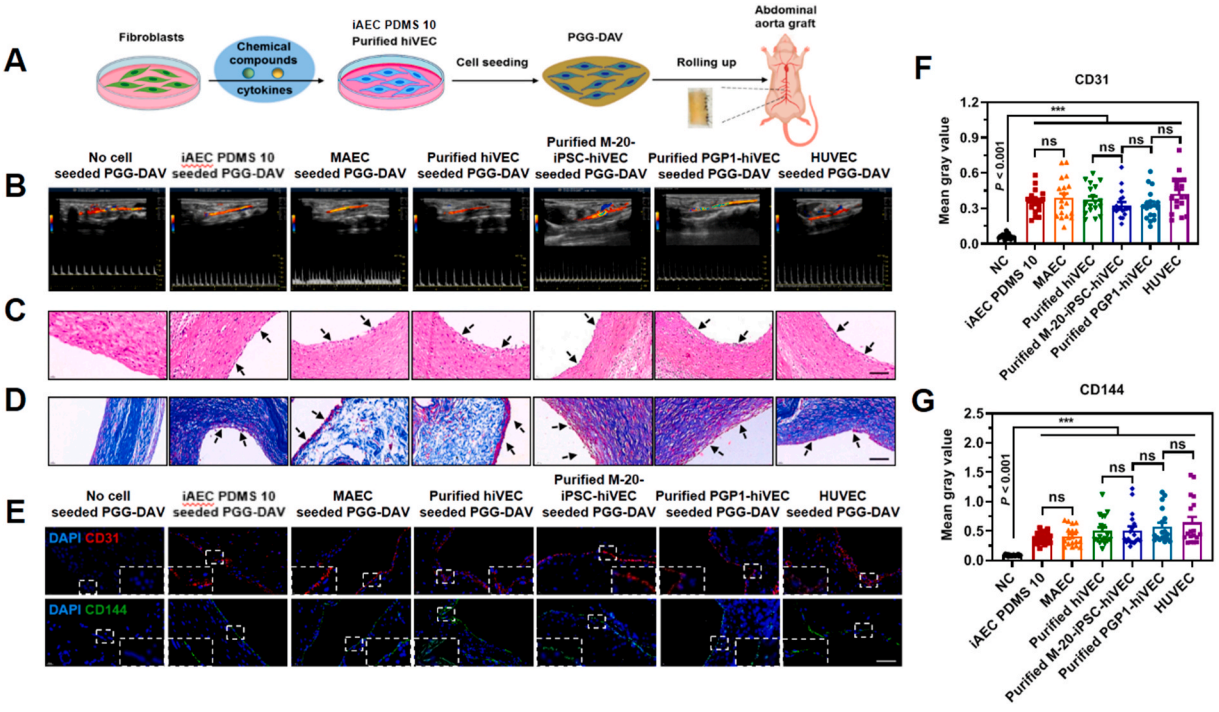

Fig. 7. iAECs and hiVECs on tissue-engineered aortic valves function for 1 month *in vivo*. (A) Schematic diagram of nude rats experiment; Rats experiment: PGG-DAV with no cells, PGG-DAV with iAEC PDMS 10, PGG-DAV with MAEC, PGG-DAV with Purified hiVEC, PGG-DAV with Purified M-20-iPSC-hiVEC, PGG-DAV with Purified PGP1-hiVEC, PGG-DAV with HUVEC cells were frizzled into tubular shape, and then transplanted to abdominal aorta of nude rats. One month later, ultrasonography was performed; subsequently the heart valves were removed out and fixed in 4 % paraformaldehyde, HE staining, and Masson's trichrome stain and immunocytochemistry were performed. (B) Representative images of ultrasonography. (C) Representative images of HE staining; Scale bar, 50 μm. (D) Representative images of Masson's trichrome stain; Scale bar, 50 μm. (E–G) Representative images and quantification of immunofluorescence of CD31, CD144; Scale bar, 50 μm; Mean ± s.e.m.; n = 18 random viewfields in 6 nude rats. Student's t-test plus Bonferroni correction or ANOVA was used for statistics. $^*P < 0.05$, $^{**}P < 0.01$, $^{***}P < 0.001$; ns = not significantly different.

3.8. iAECs and hiVECs on engineered aortic valves acquire signature of AECs or native VECs

To further investigate if the seeded iAECs or hiVECs on the aortic valve exhibit the homeostatic and coagulation inhibitory potential of the native endothelial cells, we stained P-selectin (Endothelial activation marker), E-selectin (Endothelial activation marker)), Collagen I (ECM marker), Collagen III (ECM marker), Matrix metalloproteinase13 (MMP13) (ECM degradation marker), MMP9 (ECM degradation marker), VEGFR2 (targeting the transplanted iAECs or hiVECs), α-SMA (a fibroblast marker), and NFATC1 (a VEC-specific marker) [36]. Results show that when compared with no cell seeded vascular graft, the iAECs or hiVECs exhibited cell activation with high expressions of P-selectin and E-selectin, which were like positive control HUVECs. iAECs or hiVECs seeded vascular graft had a stable ECM with high expression of Collagen I and Collagen III and low expression of MMP13 and MMP9. The transplanted iAECs or hiVECs appeared as a monolayer at the inside surface of heart valve with high expression of VEGFR2 and NFATC1 and extreme low expression of α-SMA, suggesting the transplanted iAEC or hiVECs exhibited little signs of de-differentiation (Fig. 8). The results show that there were very few lymphocytes and macrophages and a few fibroblasts were recruited from nude rats to the internal sites of the heart valve (Fig. 8 and S17G–I). The *in vivo* assessment of iAECs or hiVECs-based engineered aortic valves was prolonged to 2 months. The data show that the valves acquired the signature and the homeostatic potential of native heart valve with intact structure and appropriate functions (Fig. S18). Because there was no evidence of detachment of the implanted cells, our data suggested that it may not be likely that host cells replaced implanted cells and grew into the engineered constructs. Taken together, these results suggest that the mouse iAECs or hiVECs seeded on the decellularized aortic valves may function at least for 2 months *in vivo*.

3.9. hiVECs from transdifferentiation are safer than from iPSCs

Induced pluripotent stem cells (iPSCs) have been used as a strategy to regenerate tissue cells, which might be used as a cell source for VEC-like cells. As such, we compared cells from transdifferentiation with the cells differentiated from iPSCs. We first reprogrammed human M-20 cells into iPSCs using lentivirus and reprogramming factors according to a published method. After reprogramming, colonies of M-20-iPSCs with positive alkaline phosphatase (ALP) staining and with pluripotent stem cell markers of TRA-1-81, SSEA1, Nanog, Oct4, and Sox2 and without fibroblast markers Vimentin and S100a4 were selected and expanded (Fig. S19). In addition, we used another iPSC cell line named PGP1 (PGP1-iPSC). The two different sources of iPSCs were differentiated into hiVECs following the protocol from a recently published report [36]. Compared with the 5 % efficiency of $CD31^{+}CD144^{+}$ cells from direct transdifferentiation (hiVECs), the efficiency was 20 % for M-20-iPSC-induced VECs (iPSC-hiVECs) and 50 % for PGP1-hiVECs (Fig. S20). After MACS, the efficiency of these two methods (i.e., direct transdifferentiation and iPSC-differentiated) are similar (Fig. S21). However, since the efficiency of human fibroblast M-20 reprogramming into human iPSCs was only ~1 % (Fig. S19B) (human fibroblasts reprogramming into PGP1-iPSCs was estimated to be ~1 %), the actual efficiency of iPSC-hiVEC formation or PGP1-hiVECs (20 % of 1 %, i.e., 0.2 %, or 50 % of 1 %, i.e., 0.5 %) was 10-25-fold lower than that of the cells from direct transdifferentiation. M-20-iPSC-hiVEC and PGP1-hiVECs exhibited similar expressions of CD31 and CD144 like purified hiVECs after bioreactor assays (Fig. 6B–E) and abdominal aortic transplantation experiments (Figs. 8 and 7E-G). However, approximately 15 % of the M-20-iPSC-hiVECs and 25 % of the PGP1-hiVECs expressed a pluripotency marker Nanog (Fig. S12D), suggesting that some of these iPSC-derived hiVECs maintained undifferentiated features of stem cells. Importantly, when these cells were injected subcutaneously into NOD-SCID (Non-obese diabetic-severe combined immunodeficiency) mice, 40 % of the mice from the M-20-iPSC-hiVEC group and 80 % of the mice from the PGP1-iPSC-hiVEC group formed teratomas; in contrast, no teratoma formation was observed in the mice from the direct transdifferentiation (hiVEC) group (Fig. S22). Because it takes only a few pluripotent or multipotent undifferentiated stem cells to become tumorigenic to generate tumors, these results suggest that tumorigenesis could be a major concern for implanting iPSC-derived hiVECs, making them unsuitable for autologous tissue-engineered aortic valves.

4. Discussion

In the present study, using carefully selected soluble chemicals and growth factors and substrate stiffness that matches the native stiffness of aortic valves, we present approaches of efficiently transdifferentiating mouse fibroblasts into iAECs and human fibroblasts into hiVECs without first reprogramming them into induced pluripotent stem cells. We find that these cells express similar genes and proteins as VECs and functionally behave like VECs in culture and on decellularized porcine aortic valves. Importantly, these iAECs or hiVECs stay intact on decellularized aortic valves in bioreactors and in immune-compromised rats and could potentially serve as a cell-source for construction of autologous tissue-engineered aortic valves.

Advances from the current study over the prior art. Published reports have shown that pluripotent or multipotent stem cells can be differentiated into ECs [46,48] or heart tissues [61,62]. However, because of the potential of these stem cells in generating teratomas or tumors in the recipients, alternative strategies should be considered to bypass this critical limitation of differentiation. In our study, we have used the strategy of transdifferentiating fibroblasts into iAECs or hiVECs without first reprogramming the cells into pluripotent or multipotent stem cells. When the cells during various stages of the transdifferentiation process are assayed, no pluripotency markers of Oct4 and Nanog are expressed in those mouse or human cells, suggesting that these cells are not reprogrammed into pluripotent stem cells. In sharp contrast, when human iPSCs are differentiated into hiVECs, they express pluripotency marker Nanog and generate teratomas in NOD-SCID mice. These findings suggest that transdifferentiated cells are a better cell source for autologous tissue-engineered aortic valves than iPSCs. A study reports that heart-specific transient expression of Oct4, Sox2, Klf4, and c-Myc induces adult cardiomyocytes to dedifferentiate, which can confer regenerative capacity to adult hearts through proliferation of preexisting cardiomyocytes. However, the authors acknowledge that the possibility of tumor formation cannot be ruled out [63]. Together with our current study, these findings highlight the importance of using alternative safe approaches of direct transdifferentiation to generate autologous tissue cells. In our study, we have assessed the effect of substrate stiffness on transdifferentiation. Although published reports have shown that fibroblasts can direct transdifferentiate into endothelial cells [28–30], the strategies in those studies are to overexpress transcription factors via lentivirus. However, viral integration into the host genome increases the risk of tumorigenicity [24]. Published reports show that using lentivirus to transdifferentiate mouse fibroblasts to neural cells, an efficiency of 3 %–8 % can be achieved [64,65]. Applying a >50 % one-dimensional squeezing or compressing to the cell nucleus in a microfluidics channel [64], the efficiency is increased to ~17 %. However, it is known that applying exceptionally large mechanical deformation to the nucleus can cause DNA damage and breakage [66], leading to the potential for tumor generation, especially when virus is used in the transdifferentiation protocol. Reducing cytoskeletal tension is shown to enhance reprogramming efficiency of mouse fibroblasts into neural-like cells from ~1 % to ~6 % but lentivirus infection is used in the protocol [67]. In contrast, our protocol is free of virus and does not cause DNA damage or breakage. A published work achieves fibroblasts direct transdifferentiation into endothelial cells via chemical compounds without lentiviruses [47], but the transdifferentiation efficiency is <4 %, lower than that from our protocol. The mechanisms of each

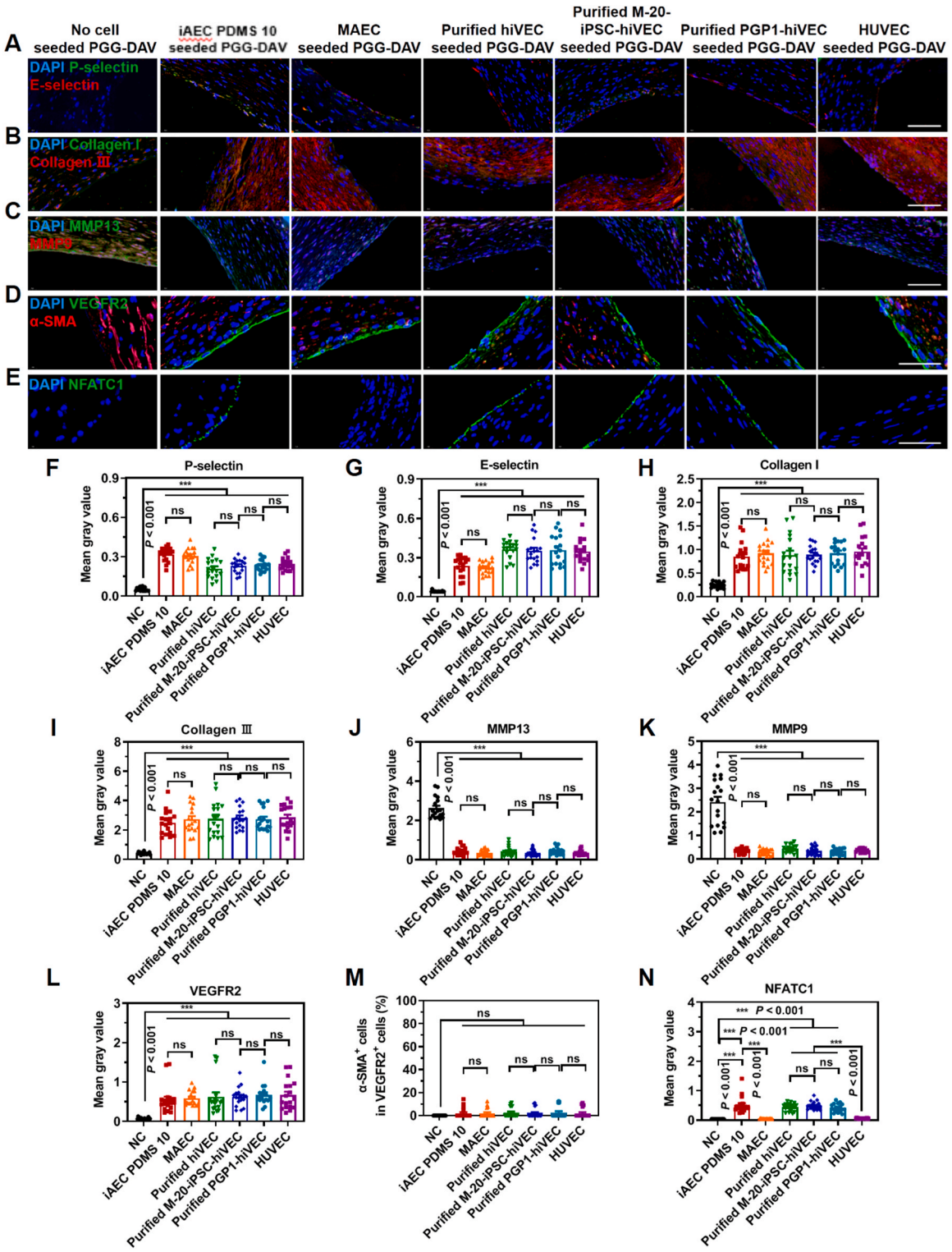

Fig. 8. iAECs and hiVECs acquire signature of AECs or native VECs for 1 month *in vivo*. Rats experiment: PGG-DAV with no cells, PGG-DAV with iAEC PDMS 10, PGG-DAV with MAEC, PGG-DAV with Purified hiVEC, PGG-DAV with Purified M-20-iPSC-hiVEC, PGG-DAV with Purified PGP1-hiVEC, PGG-DAV with HUVEC cells were frizzled into tubular shape, and then transplanted to abdominal aorta of nude rats. One month later, subsequently the heart valves were removed and fixed in 4 % paraformaldehyde, immunocytochemistry was performed. (A–E) Representative images of immunofluorescence of (A), P-selectin & E-selectin; (B) Collagen I & Collagen III; (C) MMP13 & MMP9; (D) VEGFR2 & α-SMA and (E) NFATC1. Scale bars, 50 μm. (F, G) Quantification of immunofluorescence of P-selectin and E-selectin. (H, I) Quantification of immunofluorescence of Collagen I and Collagen III. (J, K) Quantification of immunofluorescence of MMP13 and MMP9. (L, M) Quantification of immunofluorescence of VEGFR2 and the percentage of α-SMA$^+$ cells in VEGFR2$^+$ cells. (N) Quantification of immunofluorescence of NFATC1. Mean ± s.e.m.; n = 18 random viewfields in 6 nude rats. Student's t-test plus Bonferroni correction or ANOVA was used for statistics. $^*P < 0.05$, $^{**}P < 0.01$, $^{***}P < 0.001$; ns = not significantly different.

factor used in our study to induce reprogramming of fibroblasts into endothelial cells have been published extensively before. Azacytidine is a methyltransferase inhibitor which induces DNA demethylation to decondense chromatin; CHIR99021 and BMP4 promote Wnt and BMP signaling pathway activation; VEGF, DAPT, HGF, PIGF and 8-Br-cAMP promote formation and expansion of endothelial cells; SB413542 promotes maturation of endothelial cells [38,68].

PIGF and HGF promote transdifferentiation efficiency and iAEC and hiVEC maturation. Published reports have shown that PIGF (placental growth factor) can promote angiogenesis and vascular maturity of endothelial cells through Neuropilin 1 (NRP1) [69–71]. To determine whether PIGF induces VEC maturity via NRP1, we removed PIGF from the culture medium and found that there was no NRP1 phosphorylation, even when a high dose of VEGF was added (Fig. S23). However, adding PIGF back into the culture medium induced robust NRP1 phosphorylation. In addition, inhibiting VEGFR1 or VEGFR2 resulted in only a slight reduction of PIGF-induced NRP1 phosphorylation while inhibiting NRP1 completely blocked PIGF-induced NRP1 phosphorylation and NFATC1 expression (a specific VEC marker) (Fig. S23). Together, these results suggest that PIGF induces iAEC and hiVEC maturity partly through the NRP1 pathway that is independent of VEGFR1 and VEGFR2. Published reports show that HGF induces angiogenesis and endothelial cell migration [72,73].In the basic culture medium in Stage 2, cytokines such as VEGF, DAPT, PIGF and 8-Br-cAMP were included except HGF. After the cells were treated by the basic medium, the expression of p-c-Met and NFATC1 were low. After adding HGF into the basic culture medium, the expression of phosphorylated c-Met and NFATC1 increased, suggesting the important effect of HGF on the cells during transdifferentiation (Fig. S24). In addition, inhibiting c-Met decreased protein expression levels of NFATC1 and thus iAEC and hiVEC maturation (Fig. S24). Increasing the concentration of VEGF did not alter c-Met phosphorylation, suggesting that the HGF-c-Met pathway of inducing VEC maturity is independent of the VEGF pathway (Fig. S24). These results suggest that higher transdifferentiation efficiency with our protocol is due to the addition of placental growth factor (PIGF) and hepatocyte growth factor (HGF). To obtain dynamic changes of cell stage-specific transcriptional signatures, one needs to do RNA-seq and analyses at each time point and each stage, which is beyond the scope of the current study and could be explored in the future.

Appropriate substrate stiffness for high transdifferentiation efficiency. Furthermore, the use of an intermediate level of stiffness of PDMS (2.1 MPa) to maintain H3K9me3 demethylation may have facilitated activation of valvular endothelial related genes to improve transdifferentiation efficiency from mouse fibroblasts to iAECs, consistent with the published report that an intermediate substrate stiffness promotes mouse fibroblasts to neural cell differentiation [65], which shows, however, the optimal stiffness is ~20 kPa, suggesting that the optimal substrate stiffness is different for neural cells and VECs. In contrast, transdifferentiation efficiency of human embryonic fibroblasts M-20 is insensitive to substrate stiffness modulation in the presence of the soluble factors. It appears that coating of a thin layer of Matrigel on the rigid plastic yields ~5 % transdifferentiation efficiency for human embryonic fibroblasts and modulating substrate stiffness does not improve efficiency. However, human adult primary dermal fibroblasts do transdifferentiate better on 2.1 MPa PDMS substrates. The reason for the difference between human adult primary dermal fibroblasts and human embryonic fibroblasts in sensing substrate rigidity is unclear currently and deserves further investigation. A report has shown that nuclear distortion because of substrate topology by using microgrooves can facilitate reprogramming [74]. We, however, did not find improvement of transdifferentiation efficiency using similar dimensions of microgrooves, possibly because our approach is transdifferentiation that is distinct from the process of reprogramming to the pluripotent stem cells. Currently we have not tried to create valvular interstitial cells (VICs) from fibroblasts, which requires additional studies. Future studies are also needed to determine if other mechanical cues can impact and improve transdifferentiation efficiency. Nevertheless, recellularizations of decellularized aortic valves using transdifferentiated VECs and VICs are critical steps in generating next-generation tissue-engineered autologous aortic valves that can grow and regenerate to replace defective valves in patients. We acknowledge that the underlying mechanisms of the effects of substrate stiffness on transdifferentiation remain unclear. It is known that matrix stiffness regulates actin assembly and nuclear transport, modulates HAT activity and histone acetylation to open the chromatin structure that facilitates neuronal gene expression and thus enhances cell transdifferentiation [65]. Our results show that RNA Pol II S2p levels were highest at the promoter sites of Flk1, CD31, and CD144 in iAEC PDMS10 cells (Fig. S6F), suggesting that optimal substrate stiffness levels are needed for optimal transdifferentiation efficiency. More systematic studies are needed to determine the details of mechanisms of these fibroblasts transdifferentiation into iAECs and hiVECs in the future.

Limitation of the study: In the present study, we have not established a chemically defined, xeno-free system to conduct our experiments, which could limit the translational value of this study. We have used B27 and StemPro-34 media. However, induced cells that are cultured with these xeno-molecules have been used clinically and published before: B-27 containing medium with other specific cytokines has been used for culturing patients' iPSC-derived ECs [38], for culturing neural stem cells for Phase I Clinical Trial in Parkinson's Disease [75], and for expanding iPSC-derived neural stem cells and progenitor cells for being transplanted in subacute complete spinal cord injury in a first-in-human clinical trial [76,77]. StemPro-34 medium containing other cytokines has also been used for culturing human embryonic stem cell-derived cardiovascular progenitors integrated into human fetal heart tissues [78]. To limit the potential adverse effect of these xeno-molecules, we washed the cells on the decellularized porcine valve 5 times with PBS to washout the detached and loosely adhered cells before we transplanted remaining transdifferentiated iAECs or hiVECs on the porcine valve into the rat. Nevertheless, future studies are needed to establish a chemically defined, xeno-free culture system.

Another potential limitation of the study is that the NIH/3T3 mouse and M-20 human fibroblast cell lines are derived from embryos and retain multipotency. Therefore, these cells lines are not an optimal cell source for tissue engineering. We have chosen these cells lines only for the purpose of demonstrating the proof of principle and for validating our protocol. Importantly, the human primary dermal fibroblasts from adult donors that are used in this study have been shown to be able to be transdifferentiated into hiVECs, suggesting that primary adult fibroblasts from human patients are likely a good source for transdifferentiation and for seeding on decellularized porcine aortic valves for autologous transplantation into the same patients for aortic valve replacement.

No evidence of de-differentiation of mouse iAECs back to fibroblasts. After PGG-DHV incubation, on day 21, the percentage of $CD31^{+}CD144^{+}$ mouse cells are ~98 % (Fig. 1F 3rd panel and 1G), up from the 70 % at day 11. Since the total number of cells increased dramatically from day 11 to day 21, this increase in percentage of $CD31^{+}CD144^{+}$ could be due to the growth and expansion of the $CD31^{+}CD144^{+}$ cells. It is also likely that some $CD31^{+}CD144^{-}$ cells, some $CD144^{+}CD31^{-}$ cells, and/or some $CD31^{-}CD144^{-}$ turned into $CD31^{+}CD144^{+}$ cells. The percentage of $CD31^{-}CD144^{-}$ cells is only ~0.4 % (lower left corner of Fig. 1F 3rd panel shows that it is 0.34 %) after the 10 days of PGG-DHV culture. It is possible that $CD31^{-}CD144^{-}$ cells did not grow or expand at all (one could estimate that the percentage of these cells would then become ~2 % of the total cells). However, because these cells were only ~0.4 % of the total cells after 10 days of PGG-DHV culture, suggesting that some of them may turn positive for CD31, or positive for CD144, or positive for both markers, consistent with the results in Fig. 1F 3rd panel and the results that iAECs and hiVECs seeded on decellularized porcine valves are >90 % $CD144^{+}$ and $CD31^{+}$ (Fig. 6D and E) and they exhibit markers of VECs when they are

transplanted into the rat abdominal aorta (Fig. 8D and E and S18) with no signs of de-differentiation back to fibroblasts.

Transdifferentiation efficiency: The yield of human $CD31^+CD144^+$ hiVECs (~10 %) is much lower than that of mouse iAECs (~70 %) before using additional steps to increase the yield. This discrepancy may be due to the different fibroblast sources: mouse 3T3 cells are embryonic fibroblast cell lines and it is possible that they are not terminally differentiated and easier to transdifferentiate. Adult human HDF cells are primary skin fibroblasts, likely to be terminally differentiated and much more difficult to transdifferentiate. In fact, human M-20-iPSC-hiVEC and PGP1-hiVEC, both are from iPSCs, have the efficiency of ~20 % and ~50 % respectively (Figs. S20D and S20F), between the 10 % efficiency for human primary adult fibroblasts and 70 % for the mouse fibroblast cell line, supporting the notion that human primary adult terminally-differentiated fibroblasts are more difficult to trans-differentiate because of the higher landscape barrier to overcome (the Conrad Waddington landscape model). Comparisons between our transdifferentiation protocol and published papers are illustrated in Table 1. However, both M-20-iPSC-hiVEC and PGP1-hiVEC are differentiated from iPSCs, which have the risk of generating teratomas or tumors *in vivo*.

In our transdifferentiation experiments, one batch of human adult primary dermal fibroblasts (a total of seeded cells of $1.06x10^6$ at day 0) grew to $95x10^6$ cells at day 13. After MACS, there were $9x10^6$ cells remaining, enough to seed 100 porcine valves (each porcine valve was seeded with $0.9x10^5$ cells) (a porcine valve had a surface area of 4 cm^2, like a 3-cm^2 human adult aortic valve [79]. By day 20, a total of $70x10^6$ hiVECs were recovered, resulting in a transdifferentiation yield of ~66-fold (70 divided by 1.06) (Table S5). However, not all 100-hiVEC--seeded porcine valves are needed for transplantation. For autologous transplantation, one patient only needs one hiVEC-seeded porcine valve to be sutured that matches the size of the patient's valve, although several porcine valves may be needed for the proper seeding and size matching. Therefore, our protocol is sufficient to generate enough engineered valves to meet the need of the patient. The autologous fibroblasts from this patient from one biopsy (~1 million cells), even with the low yield of ~10 %, can be expanded to 70 million hiVECs (after sorting and PGG-DHV culture), which are enough to seed many porcine valves for transplantation. It is anticipated that the majority of hiVECs will be thrown away after the valve replacement because these extra cells on PGG-DHV are not suitable for other aortic valve patients due to immune rejection. Thus, the low yield of hiVECs is not a limiting factor in aortic valve replacement. In addition, our protocol is not labor-intensive nor costly because using our protocol one graduate student can transdifferentiate human primary adult fibroblasts into hiVECs on decellularized porcine valves in 20 days.

Future directions. At the present time, we are not able to implant the engineered aortic valves at the site of the aortic valve of an animal model because we are not able to find an immune-compromised animal that is large enough in size to be operated on to replace the native valve. Nevertheless, it will be interesting to examine if it is possible to use immune-competent large animals as animal models and treat them with immuno-suppressing drugs and then implant these engineered aortic valves seeding with mouse or human cells into the heart of these animals as prosthetic aortic valves. With the recent advance of technology in 3D-printing heart tissues [32], it will be interesting to determine in the future if it is possible to use our protocol to produce and to seed autologous hiVECs onto a 3D-printed aortic valve to generate a functional tissue-engineered human aortic valve.

Table 1
Comparisons among various protocols.

Reference	Category	Cell resource	Protocol	Efficiency
[28]	Transdifferentiation to induced endothelial cells (ECs)	Human neonatal fibroblasts	Virus vectors + Transcription factors + Cytokines + Small molecules	3.9 %
[29]	Transdifferentiation to ECs	Human postnatal dermal fibroblasts	Virus vectors + Transcription factors + Cytokines	12 %–15 %
[47]	Transdifferentiation to ECs	Human foreskin fibroblasts	Cytokines + Small molecules	3.9 %
[64]	Transdifferentiation to neuronal cells	Mouse fibroblast	Virus vectors + Transcription factors + Mechanical force	15 %
[65]	Transdifferentiation to neuronal cells	Mouse fibroblast	Virus vectors + Transcription factors + Substrate stiffness	8 %
[67]	Transdifferentiation to induced neural cells	Mouse fibroblast	Virus vectors + Transcription factors + Cytokines + Mechanical manipulation	4 %
Current study	Transdifferentiation to iAECs and hiVECs	Mouse fibroblast and primary human dermal fibroblast	Cytokines + Small molecules + Substrate stiffness	iAECs: ~70 % hiVECs: ~10 %

5. Conclusion

In summary, we report here a strategy to directly convert differentiated fibroblasts into iAECs or hiVECs without virus utilization and genetic manipulation. Utilizing a combinatorial strategy of selective soluble chemicals, cytokines and substrate stiffness modulation, mouse embryonic fibroblasts are directly and efficiently transdifferentiated into induced aortic endothelial cell-like cells (iAECs) and human primary adult fibroblasts are transdifferentiated into induced valvular endothelial cell-like cells. These cells show VEC-associated markers and functions. The iAECs or hiVECs seeded on decellularized porcine aortic valves stay intact and express VEC-associated proteins for 60 days *in vivo*. In contrast, induced pluripotent stem cells (iPSCs) are less efficient in differentiating into hiVECs, iPSC-derived hiVECs generate teratomas *in vivo*. Our findings highlight an approach to efficiently convert fibroblasts into iAEC or hiVECs and seed them onto decellularized aortic valves for safely generating autologous tissue-engineered aortic valves.

CRediT authorship contribution statement

Peng Tang: Writing – original draft, Methodology, Investigation. **Fuxiang Wei:** Writing – original draft, Methodology, Investigation. **Weihua Qiao:** Writing – original draft, Methodology, Investigation. **Xing Chen:** Investigation. **Chenyang Ji:** Investigation. **Wanzhi Yang:** Investigation. **Xinyu Zhang:** Investigation. **Sihan Chen:** Investigation. **Yanyan Wu:** Investigation. **Mingxing Jiang:** Investigation. **Chenyu Ma:** Investigation. **Weiqiang Shen:** Investigation. **Qi Dong:** Investigation. **Hong Cao:** Investigation. **Minghui Xie:** Investigation. **Ziwen Cai:** Investigation. **Li Xu:** Investigation. **Jiawei Shi:** Investigation. **Nianguo Dong:** Writing – review & editing, Supervision, Project administration, Methodology, Funding acquisition. **Junwei Chen:** Writing – review & editing, Supervision, Project administration, Methodology, Funding acquisition. **Ning Wang:** Writing – review & editing, Supervision, Project administration, Methodology, Funding acquisition.

Data availability

The data that support the findings of this study are available from the corresponding author upon reasonable request. The RNA-seq data are deposited at Genome Sequence Archive (GSA) database: https://ngdc.cncb.ac.cn/gsa-human/s/4zk2gtT0 or https://ngdc.cncb.ac.cn/gsa-human (access number: HRA005410).

Ethics approval and consent to participate

All animals received humane care in compliance with the Principles of Laboratory All animals received humane care in compliance with the Principles of Laboratory Animal Care Formulated by the National Society of Medical Research and the Guide for the Care and Use of Laboratory Animals by National Research Council (US). The protocol was approved by the Animal Care and Use Committee of Huazhong University of Science and Technology.

Declaration of competing interest

The authors declare that they have no known competing financial interests or personal relationships that could have appeared to influence the work reported in this paper.

Acknowledgments

We thank Dr. Shao Yue for providing the PDMS and Dr. Yuhua Sun for providing PGP1 iPSCs. We thank Wuhan Onemore-tech Co., Ltd. for their assistance with sequencing and RNA-seq analysis. All cell culture experiments were performed at Life Science College and bioreactor experiments and rat experiments were performed at Tongji Medical College. This study was a collaboration between the lab of JC and the lab of ND and the collaboration was limited to this project only. This work was supported by the Ministry of Science and Technology of China grants 2021YFA1101900 (ND), National Natural Science Foundation of China grants (12422212,32071306,11902121) (JC), Huazhong University of Science and Technology Program for Academic Frontier Youth Team grant (2018QYTD01) (JC), the Fundamental Research Funds for the Central Universities (2024BRB004) (JC), USA National Institutes of Health grant R01 GM072744 (NW), Northeastern University in Boston (NW).

Appendix A. Supplementary data

Supplementary data to this article can be found online at https://doi.org/10.1016/j.bioactmat.2024.11.018.

References

[1] M.H. Yacoub, J.J. Takkenberg, Will heart valve tissue engineering change the world? Nat. Clin. Pract. Cardiovasc. Med. 2 (2) (2005) 60–61.
[2] J.L. d'Arcy, B.D. Prendergast, J.B. Chambers, S.G. Ray, B. Bridgewater, Valvular heart disease: the next cardiac epidemic, Heart 97 (2) (2011) 91–93.
[3] A.K. Capulli, M.Y. Emmert, F.S. Pasqualini, D. Kehl, E. Caliskan, J.U. Lind, S. P. Sheehy, S.J. Park, S. Ahn, B. Weber, J.A. Goss, S.P. Hoerstrup, K. K, JetValve: rapid manufacturing of biohybrid scaffolds for biomimetic heart valve replacement, Biomaterials 133 (2017) 229–241.
[4] C.V. Bouten, A. Driessen-Mol, F.P. Baaijens, In situ heart valve tissue engineering: simple devices, smart materials, complex knowledge, Expet Rev. Med. Dev. 9 (5) (2012) 453–455.
[5] E.S. Fioretta, S.E. Motta, V. Lintas, S. Loerakker, K.K. Parker, F.P.T. Baaijens, V. Falk, S.P. Hoerstrup, M.Y. Emmert, Next-generation tissue-engineered heart valves with repair, remodelling and regeneration capacity, Nat. Rev. Cardiol. 18 (2) (2021) 92–116.
[6] S.P. Nejad, M.C. Blaser, J.P. Santerre, C.A. Caldarone, C.A. Simmons, Biomechanical conditioning of tissue engineered heart valves: too much of a good thing? Adv. Drug Deliv. Rev. 96 (2016) 161–175.
[7] B.A. Aguado, K.B. Schuetze, J.C. Grim, C.J. Walker, A.C. Cox, T.L. Ceccato, A. C. Tan, C.C. Sucharov, L.A. Leinwand, M.R.G. Taylor, T.A. McKinsey, K.S. Anseth, Transcatheter aortic valve replacements alter circulating serum factors to mediate myofibroblast deactivation, Sci. Transl. Med. 11 (509) (2019) eaav3233.
[8] J.C. Grim, B.A. Aguado, B.J. Vogt, D. Batan, C.L. Andrichik, M.E. Schroeder, A. Gonzalez-Rodriguez, F.M. Yavitt, R.M. Weiss, K.S. Anseth, Secreted factors from proinflammatory macrophages promote an osteoblast-like phenotype in valvular interstitial cells, Arterioscler. Thromb. Vasc. Biol. 40 (11) (2020) e296–e308.
[9] R.S. Farivar, L.H. Cohn, E.G. Soltesz, T. Mihaljevic, J.D. Rawn, J.G. Byrne, Transcriptional profiling and growth kinetics of endothelium reveals differences between cells derived from porcine aorta versus aortic valve, Eur. J. Cardio. Thorac. Surg. 24 (4) (2003) 527–534.
[10] J.D. Deck, Endothelial cell orientation on aortic valve leaflets, Cardiovasc. Res. 20 (10) (1986) 760–767.
[11] C.A. Simmons, G.R. Grant, E. Manduchi, P.F. Davies, Spatial heterogeneity of endothelial phenotypes correlates with side-specific vulnerability to calcification in normal porcine aortic valves, Circ. Res. 96 (7) (2005) 792–799.
[12] C.J. Holliday, R.F. Ankeny, H. Jo, R.M. Nerem, Discovery of shear- and side-specific mRNAs and miRNAs in human aortic valvular endothelial cells, Am. J. Physiol. Heart Circ. Physiol. 301 (3) (2011) H856–H867.
[13] M.C. VeDepo, M.S. Detamore, R.A. Hopkins, G.L. Converse, Recellularization of decellularized heart valves: progress toward the tissue-engineered heart valve, J. Tissue Eng. 8 (2017).
[14] J. Dai, W. Qiao, J. Shi, C. Liu, X. Hu, N. Dong, Modifying decellularized aortic valve scaffolds with stromal cell-derived factor-1α loaded proteolytically degradable hydrogel for recellularization and remodeling, Acta Biomater. 88 (2019) 280–292.
[15] K. Takahashi, K. Okita, M. Nakagawa, S. Yamanaka, Induction of pluripotent stem cells from fibroblast cultures, Nat. Protoc. 2 (12) (2007) 3081–3089.
[16] K. Takahashi, S. Yamanaka, Induction of pluripotent stem cells from mouse embryonic and adult fibroblast cultures by defined factors, Cell 126 (4) (2006) 663–676.
[17] K. Okita, M. Nakagawa, H. Hyenjong, T. Ichisaka, S. Yamanaka, Generation of mouse induced pluripotent stem cells without viral vectors, Science 322 (5903) (2008) 949–953.
[18] J. Yu, M.A. Vodyanik, K. Smuga-Otto, J. Antosiewicz-Bourget, J.L. Frane, S. Tian, J. Nie, G.A. Jonsdottir, V. Ruotti, R. Stewart, Induced pluripotent stem cell lines derived from human somatic cells, Science 318 (5858) (2007) 1917–1920.
[19] T. Takebe, K. Sekine, M. Enomura, H. Koike, M. Kimura, T. Ogaeri, R.R. Zhang, Y. Ueno, Y.W. Zheng, N. Koike, Vascularized and functional human liver from an iPSC-derived organ transplant, Nature 499 (7459) (2013) 481–484.
[20] Y. Shiba, T. Gomibuchi, T. Seto, Y. Wada, H. Ichimura, Y. Tanaka, T. Ogasawara, K. Okada, N. Shiba, K. Sakamoto, Allogeneic transplantation of iPS cell-derived cardiomyocytes regenerates primate hearts, Nature 538 (7625) (2016) 388–391.
[21] J. Strnadel, C. Carromeu, C. Bardy, M. Navarro, O. Platoshyn, A.N. Glud, S. Marsala, J. Kafka, A. Miyanohara, T. Kato, Survival of syngeneic and allogeneic iPSC-derived neural precursors after spinal grafting in minipigs, Sci. Transl. Med. 10 (440) (2018) eaam6651.
[22] M. Gu, N.Y. Shao, S. Sa, D. Li, V. Termglinchan, M. Ameen, I. Karakikes, G. Sosa, F. Grubert, J. Lee, Patient-specific iPSC-derived endothelial cells uncover pathways that protect against pulmonary hypertension in BMPR2 mutation carriers, Cell Stem Cell 20 (4) (2017) 490–504.
[23] D.E. Cohen, D.A. Melton, Turning straw into gold: directing cell fate for regenerative medicine, Nat. Rev. Genet. 12 (4) (2011) 243–252.
[24] P.S. Knoepfler, Deconstructing stem cell tumorigenicity: a roadmap to safe regenerative medicine, Stem Cell. 27 (5) (2009) 1050–1056.
[25] S. Yamanaka, A fresh look at iPS cells, Cell 137 (1) (2009) 13–17.
[26] Q. Zhou, J. Brown, A. Kanarek, J. Rajagopal, D.A. Melton, In vivo reprogramming of adult pancreatic exocrine cells to beta-cells, Nature 455 (7213) (2008) 627–632.
[27] M. Ginsberg, D. James, B.S. Ding, D. Nolan, F. Geng, J.M. Butler, W. Schachterle, V. R. Pulijaal, S. Mathew, S.T. Chasen, Efficient direct reprogramming of mature amniotic cells into endothelial cells by ETS factors and TGFβ suppression, Cell 151 (3) (2012) 559–575.
[28] J. Li, N.F. Huang, J. Zou, T.J. Laurent, J.C. Lee, J. Okogbaa, J.P. Cooke, S. Ding, Conversion of human fibroblasts to functional endothelial cells by defined factors, Arterioscler. Thromb. Vasc. Biol. 33 (6) (2013) 1366–1375.
[29] S. Lee, C. Park, J.W. Han, J.Y. Kim, K. Cho, E.J. Kim, S. Kim, S.J. Lee, S.Y. Oh, Y. Tanaka, Direct reprogramming of human dermal fibroblasts into endothelial cells using ER71/ETV2, Circ. Res. 120 (5) (2017) 848–861.
[30] S. Cho, P. Aakash, S. Lee, Y.S. Yoon, Endothelial cell direct reprogramming: past, present, and future, J. Mol. Cell. Cardiol. 180 (2023) 22–32.
[31] H. Cao, Q. Zhou, C. Liu, Y. Zhang, M. Xie, W. Qiao, N. Dong, Substrate stiffness regulates differentiation of induced pluripotent stem cells into heart valve endothelial cells, Acta, Biomater 143 (2022) 115–126.
[32] S. Choi, K.Y. Lee, S.L. Kim, L.A. MacQueen, H. Chang, J.F. Zimmerman, Q. Jin, M. M. Peters, H.A.M. Ardoña, X. Liu, A.C. Heiler, R. Gabardi, C. Richardson, W.T. Pu, A.R. Bausch, K.K. Parker, Fibre-infused gel scaffolds guide cardiomyocyte alignment in 3D-printed ventricles, Nat. Mater. 22 (8) (2023) 1039–1046.
[33] Y. Rinkevich, G.G. Walmsley, M.S. Hu, Z.N. Maan, A.M. Newman, M. Drukker, M. Januszyk, G.W. Krampitz, G.C. Gurtner, H.P. Lorenz, Skin fibrosis. Identification and isolation of a dermal lineage with intrinsic fibrogenic potential, Science 348 (6232) (2015) aaa2151.
[34] F. Chowdhury, S. Na, D. Li, Y.C. Poh, T.S. Tanaka, F. Wang, N. Wang, Material properties of the cell dictate stress-induced spreading and differentiation in embryonic stem cells, Nat. Mater. 9 (1) (2010) 82–88.
[35] Y. Zhao, X. Yin, H. Qin, F. Zhu, H. Liu, W. Yang, Q. Zhang, C. Xiang, P. Hou, Z. Song, Two supporting factors greatly improve the efficiency of human iPSC generation, Cell Stem Cell 3 (5) (2008) 475–479.
[36] L. Cheng, M. Xie, W. Qiao, Y. Song, Y. Zhang, Y. Geng, W. Xu, L. Wang, Z. Wang, K. Huang, Generation and characterization of cardiac valve endothelial-like cells from human pluripotent stem cells, Commun, Biol. 4 (1) (2021) 1039.

[37] F. Song, D. Ren, Stiffness of cross-linked poly(dimethylsiloxane) affects bacterial adhesion and antibiotic susceptibility of attached cells, Langmuir 30 (34) (2014) 10354–10362.
[38] N. Sayed, C. Liu, M. Ameen, F. Himmati, J.Z. Zhang, S. Khanamiri, J.R. Moonen, A. Wnorowski, L. Cheng, J.W. Rhee, Clinical trial in a dish using iPSCs shows lovastatin improves endothelial dysfunction and cellular crosstalk in LMNA cardiomyopathy, Sci. Transl. Med. 12 (554) (2020) eaax9276.
[39] K. Sugihara, Y. Yamaguchi, S. Usui, Y. Nashimoto, S. Hanada, E. Kiyokawa, A. Uemura, R. Yokokawa, K. Nishiyama, T. Miura, A new perfusion culture method with a self-organized capillary network, PLoS One 15 (10) (2020) e0240552.
[40] D. Merrick, A. Sakers, Z. Irgebay, C. Okada, C. Calvert, M.P. Morley, I. Percec, P. Seale, Identification of a mesenchymal progenitor cell hierarchy in adipose tissue, Science 364 (6438) (2019) eaav2501.
[41] W.H. Qiao, P. Liu, D. Hu, M. Al Shirbini, X.M. Zhou, N.G. Dong, Sequential hydrophile and lipophile solubilization as an efficient method for decellularization of porcine aortic valve leaflets: structure, mechanical property and biocompatibility study, J. Tissue Eng. Regen. Med. 12 (2) (2018) e828–e840.
[42] L.N. Sierad, A. Simionescu, C. Albers, J. Chen, J. Maivelett, M.E. Tedder, J. Liao, D. T. Simionescu, Design and testing of a pulsatile conditioning system for dynamic endothelialization of polyphenol-stabilized tissue engineered heart valves, Cardiovasc. Eng. Technol. 1 (2) (2010) 138–153.
[43] U.M. Vischer, D.D. Wagner, CD63 is a component of Weibel-Palade bodies of human endothelial cells, Blood 82 (4) (1993) 1184–1191.
[44] M. Groudine, R. Eisenman, H. Weintraub, Chromatin structure of endogenous retroviral genes and activation by an inhibitor of DNA methylation, Nature 292 (5821) (1981) 311–317.
[45] G. Pennarossa, S. Maffei, M. Campagnol, L. Tarantini, F. Gandolfi, T.A. Brevini, Brief demethylation step allows the conversion of adult human skin fibroblasts into insulin-secreting cells, Proc. Natl. Acad. Sci. U.S.A. 110 (22) (2013) 8948–8953.
[46] M. Sahara, E.M. Hansson, O. Wernet, K.O. Lui, D. Später, K.R. Chien, Manipulation of a VEGF-Notch signaling circuit drives formation of functional vascular endothelial progenitors from human pluripotent stem cells, Cell Res. 24 (7) (2014) 820–841.
[47] N. Sayed, W.T. Wong, F. Ospino, S. Meng, J. Lee, A. Jha, P. Dexheimer, B. J. Aronow, J.P. Cooke, Transdifferentiation of human fibroblasts to endothelial cells: role of innate immunity, Circulation 131 (3) (2015) 300–309.
[48] G. Arderiu, E. Peña, R. Aledo, O. Juan-Babot, J. Crespo, G. Vilahur, B. Oñate, F. Moscatiello, L. Badimon, MicroRNA-145 regulates the differentiation of adipose stem cells toward microvascular endothelial cells and promotes angiogenesis, Circ. Res. 125 (1) (2019) 74–89.
[49] A.J. Engler, S. Sen, H.L. Sweeney, D.E. Discher, Matrix elasticity directs stem cell lineage specification, Cell 126 (4) (2006) 677–689.
[50] A. Hasan, K. Ragaert, W. Swieszkowski, S. Selimović, A. Paul, G. Camci-Unal, M. R. Mofrad, A. Khademhosseini, Biomechanical properties of native and tissue engineered heart valve constructs, J. Biomech. 47 (9) (2014) 1949–1963.
[51] R.A. Gould, J.T. Butcher, Isolation of valvular endothelial cells, J. Vis. Exp. 46 (2010) 2158.
[52] N. Yosef, R.H. Xia, E.E. Ubogu, Development and characterization of a novel human in vitro blood-nerve barrier model using primary endoneurial endothelial cells, J. Neuropathol, Exp. Neurol. 69 (1) (2010) 82–97.
[53] F. Chalajour, H. Treede, A. Ebrahimnejad, H. Lauke, H. Reichenspurner, S. Ergun, Angiogenic activation of valvular endothelial cells in aortic valve stenosis, Exp. Cell Res. 298 (2) (2004) 455–464.
[54] E. Ubil, J. Duan, I. Pillai, M. Rosa-Garrido, Y. Wu, F. Bargiacchi, Y. Lu, S. Stanbouly, J. Huang, M. Rojas, Mesenchymal-endothelial transition contributes to cardiac neovascularization, Nature 514 (7524) (2014) 585–590.
[55] Y.M. Meng, X. Jiang, X. Zhao, Q. Meng, S. Wu, Y. Chen, X. Kong, X. Qiu, L. Su, C. Huang, Hexokinase 2-driven glycolysis in pericytes activates their contractility leading to tumor blood vessel abnormalities, Nat. Commun. 12 (1) (2021) 6011.
[56] A. Belyaeva, S. Venkatachalapathy, M. Nagarajan, G.V. Shivashankar, C. Uhler, Network analysis identifies chromosome intermingling regions as regulatory hotspots for transcription, Proc. Natl. Acad. Sci. U.S.A. 114 (52) (2017) 13714–13719.
[57] J. Sun, J. Chen, E. Mohagheghian, N. Wang, Force-induced gene up-regulation does not follow the weak power law but depends on H3K9 demethylation, Sci. Adv. 6 (14) (2020) eaay9095.
[58] Y. Kalukula, A.D. Stephens, J. Lammerding, S. Gabriele, Mechanics and functional consequences of nuclear deformations, Nat. Rev. Mol. Cell Biol. 23 (9) (2022) 583–602.
[59] D. James, H.S. Nam, M. Seandel, D. Nolan, T. Janovitz, M. Tomishima, L. Studer, G. Lee, D. Lyden, R. Benezra, Expansion and maintenance of human embryonic stem cell-derived endothelial cells by TGFbeta inhibition is Id1 dependent, Nat. Biotechnol. 28 (2) (2010) 161–166.
[60] M. Boulberdaa, E. Scott, M. Ballantyne, R. Garcia, B. Descamps, G.D. Angelini, M. Brittan, A. Hunter, M. McBride, J. McClure, A role for the long noncoding RNA SENCR in commitment and function of endothelial cells, Mol. Ther. 24 (5) (2016) 978–990.
[61] J. Riegler, M. Tiburcy, A. Ebert, E. Tzatzalos, U. Raaz, O.J. Abilez, Q. Shen, N. G. Kooreman, E. Neofytou, V.C. Chen, Human engineered heart muscles engraft and survive long term in a rodent myocardial infarction model, Circ. Res. 117 (8) (2015) 720–730.
[62] I. Goldfracht, S. Protze, A. Shiti, N. Setter, A. Gruber, N. Shaheen, Y. Nartiss, G. Keller, L. Gepstein, Generating ring-shaped engineered heart tissues from ventricular and atrial human pluripotent stem cell-derived cardiomyocytes, Nat. Commun. 11 (1) (2020) 75.
[63] Y. Chen, F.F. Lüttmann, E. Schoger, H.R. Schöler, L.C. Zelarayán, K.P. Kim, J. J. Haigh, J. Kim, T. Braun, Reversible reprogramming of cardiomyocytes to a fetal state drives heart regeneration in mice, Science 373 (6562) (2021) 1537–1540.
[64] Y. Song, J. Soto, B. Chen, T. Hoffman, W. Zhao, N. Zhu, Q. Peng, L. Liu, C. Ly, P. K. Wong, Y. Wang, A.C. Rowat, S.K. Kurdistani, S. Li, Transient nuclear deformation primes epigenetic state and promotes cell reprogramming, Nat. Mater. 21 (10) (2022) 1191–1199.
[65] Y. Song, J. Soto, S.Y. Wong, Y. Wu, T. Hoffman, N. Akhtar, S. Norris, J. Chu, H. Park, D.O. Kelkhoff, Biphasic regulation of epigenetic state by matrix stiffness during cell reprogramming, Sci. Adv. 10 (7) (2024) eadk0639.
[66] S. Cho, M. Vashisth, A. Abbas, S. Majkut, K. Vogel, Y. Xia, I.L. Ivanovska, J. Irianto, M. Tewari, K. Zhu, Mechanosensing by the lamina protects against nuclear rupture, DNA damage, and cell-cycle arrest, Dev. Cell 49 (6) (2019) 920–935.
[67] J. Soto, Y. Song, Y. Wu, B. Chen, H. Park, N. Akhtar, P.Y. Wang, T. Hoffman, C. Ly, J. Sia, S. Wong, D.O. Kelkhoff, J. Chu, M.M. Poo, T.L. Downing, A.C. Rowat, S. Li, Reduction of intracellular tension and cell adhesion promotes open chromatin structure and enhances cell reprogramming, Adv. Sci. 10 (24) (2023) e2300152.
[68] J. Nguyen, Y.Y. Lin, S. Gerecht, The next generation of endothelial differentiation: tissue-specific ECs, Cell Stem Cell 28 (7) (2021) 1188–1204.
[69] M. Migdal, B. Huppertz, S. Tessler, A. Comforti, M. Shibuya, R. Reich, H. Baumann, G. Neufeld, Neuropilin-1 is a placenta growth factor-2 receptor, J. Biol. Chem. 273 (35) (1998) 22272–22278.
[70] Z. Lyu, H. Jin, Z. Yan, K. Hu, H. Jiang, H. Peng, H. Zhuo, Effects of NRP1 on angiogenesis and vascular maturity in endothelial cells are dependent on the expression of SEMA4D, Int. J. Mol. Med. 46 (4) (2020) 1321–1334.
[71] M. Klagsbrun, S. Takashima, R. Mamluk, The role of neuropilin in vascular and tumor biology, Adv. Exp. Med. Biol. 515 (2002) 33–48.
[72] M. Manganini, J. Maier, Transforming growth factor beta2 inhibition of hepatocyte growth factor-induced endothelial proliferation and migration, Oncogene 19 (1) (2000) 124–133.
[73] M. Aoki, R. Morishita, Y. Taniyama, I. Kida, A. Moriguchi, K. Matsumoto, T. Nakamura, Y. Kaneda, J. Higaki, T. Ogihara, Angiogenesis induced by hepatocyte growth factor in non-infarcted myocardium and infarcted myocardium: up-regulation of essential transcription factor for angiogenesis, ets, Gene Ther. 7 (5) (2000) 417–427.
[74] T.L. Downing, J. Soto, C. Morez, T. Houssin, A. Fritz, F. Yuan, J. Chu, S. Patel, D. V. Schaffer, S. Li, Biophysical regulation of epigenetic state and cell reprogramming, Nat. Mater. 12 (12) (2013) 1154–1162.
[75] I. Garitaonandia, R. Gonzalez, T. Christiansen-Weber, T. Abramihina, M. Poustovoitov, A. Noskov, G. Sherman, A. Semechkin, E. Snyder, R. Kern, Neural stem cell tumorigenicity and biodistribution assessment for Phase I clinical trial in Parkinson's disease, Sci. Rep. 6 (2016) 34478.
[76] K. Sugai, M. Sumida, T. Shofuda, R. Yamaguchi, T. Tamura, T. Kohzuki, T. Abe, R. Shibata, Y. Kamata, S. Ito, First-in-human clinical trial of transplantation of iPSC-derived NS/PCs in subacute complete spinal cord injury: study protocol, Regen. Ther. 18 (2021) 321–333.
[77] Y. Kanemura, H. Mori, S. Kobayashi, O. Islam, E. Kodama, A. Yamamoto, Y. Nakanishi, N. Arita, M. Yamasaki, H. Okano, Evaluation of in vitro proliferative activity of human fetal neural stem/progenitor cells using indirect measurements of viable cells based on cellular metabolic activity, J. Neurosci. Res. 69 (6) (2002) 869–879.
[78] R. Ardehali, S.R. Ali, M.A. Inlay, O.J. Abilez, M.Q. Chen, T.A. Blauwkamp, M. Yazawa, Y. Gong, R. Nusse, M. Drukker, Prospective isolation of human embryonic stem cell-derived cardiovascular progenitors that integrate into human fetal heart tissue, Proc. Natl. Acad. Sci. U.S.A. 110 (9) (2013) 3405–3410.
[79] A.C. Pouleur, J.B. le Polain de Waroux, A. Pasquet, J.L. Vanoverschelde, B. L. Gerber, Aortic valve area assessment: multidetector CT compared with cine MR imaging and transthoracic and transesophageal echocardiography, Radiology 244 (3) (2007) 745–754.